MIT Libraries | DSpace@MIT

MIT Open Access Articles

Precise mapping of the magnetic field in the CMS barrel yoke using cosmic rays

Massachusetts Institute of Technology

CMS Paper

arXiv:0910.5530v2 [physics.ins-det] 4 Jan 2010

Precise Mapping of the Magnetic Field in the CMS Barrel Yoke using Cosmic Rays

The CMS Collaboration*

Abstract

The CMS detector is designed around a large 4 T superconducting solenoid, enclosed in a 12 000-tonne steel return yoke. A detailed map of the magnetic field is required for the accurate simulation and reconstruction of physics events in the CMS detector, not only in the inner tracking region inside the solenoid but also in the large and complex structure of the steel yoke, which is instrumented with muon chambers. Using a large sample of cosmic muon events collected by CMS in 2008, the field in the steel of the barrel yoke has been determined with a precision of 3 to 8% depending on the location.

*See Appendix A for the list of collaboration members

1 Introduction

The Compact Muon Solenoid (CMS) [1] is a general-purpose detector whose main goal is to explore physics at the TeV scale by exploiting the proton-proton collisions provided by the Large Hadron Collider (LHC) [2] at CERN. Its distinctive features include a 4 T superconducting solenoid with a free bore of a diameter of 6 m and a length of 12.5 m, enclosed inside a 12 000-tonne yoke made of common structural steel [3]. The geometry of CMS is shown in Fig. 1. The yoke is composed of five three-layered dodecagonal barrel wheels and three endcap disks at each end. In the barrel region the innermost yoke layer is 295 mm thick and each of the two outermost ones is 630 mm thick. The yoke contributes to only 8% of the central magnetic flux density; its main role is to increase the field homogeneity in the tracker volume and to reduce the stray field by returning the magnetic flux of the solenoid. In addition, the steel plates play the role of absorber for the four interleaved layers ("stations") of muon chambers, which provide for a measurement of the muon momentum independent of the inner tracking system.
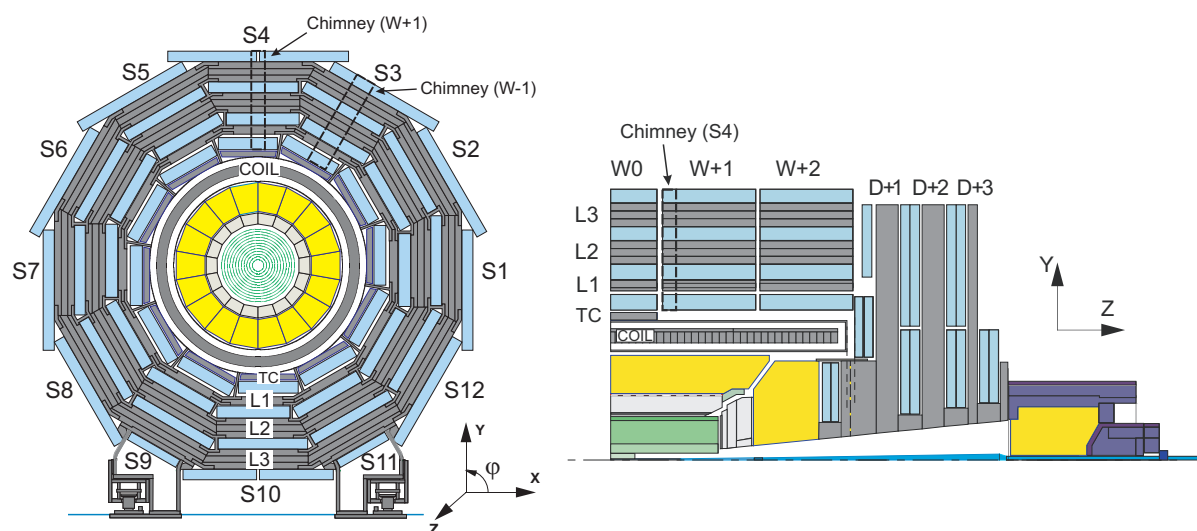

Figure 1: Schematic views of the CMS detector, with the numbering convention for azimuthal sectors (S), wheels (W), barrel yoke layers (L) and endcap disks (D). "TC" is the "tail catcher", an additional steel layer present in the central barrel wheel only. Left: transverse view at $z = 0$. Right: longitudinal view of one quarter of the detector. Wheels on the $z < 0$ side (not shown) are labeled W-1 and W-2. The location of the "chimneys" described in Section 3 is indicated with boxes.

The CMS collaboration has decided to operate the magnet at a central magnetic flux density of 3.8 T. After the first years of operation, once the aging of the coil is better understood, the collaboration may decide to operate the magnet at 4 T.

In order to allow accurate reconstruction of track parameters and Monte Carlo simulation of events, a detailed map of the magnetic field in the entire volume of the CMS detector is needed. The accuracy of the magnetic field map is discussed in Section 2. Sections 3 and 4 describe the computation of the CMS field map and its implementation in the CMS software framework, respectively.

Several techniques have been adopted to directly measure and to monitor the magnetic flux density B in the various parts of the CMS detector, as discussed in Section 5. In particular, the field in the central volume of the solenoid was mapped with very good precision. However, measurements with probes outside the solenoid are not sufficient to constrain the field map

inside the steel of the yoke to the level of precision required.

During October-November 2008, the CMS Collaboration conducted a month-long data-taking exercise known as the Cosmic Run At Four Tesla (CRAFT), with the goal of commissioning the experiment for extended operation [4]. With all installed detector systems participating, CMS recorded 270 million cosmic ray triggered events with the solenoid at a central magnetic flux density of 3.8 T. Using these data it was possible for the first time to probe the magnetic field in the steel of the return yoke using reconstructed muon tracks. The field in the different parts of the barrel yoke was measured and correction factors for the field map were obtained, as described in Section 6.

This paper does not cover the study of the field in the endcap yoke. That analysis is more challenging, since the number of cosmic muons traversing both the inner tracker and the endcap stations is limited for geometrical reasons.

2   Accuracy of the Magnetic Field Map

The CMS silicon tracker, the central detector for charged particle track reconstruction, is located centrally inside the superconducting coil of the magnet of the CMS detector. Within that region, the field has a high strength and is relatively homogeneous. As discussed in Section 5, the field in the tracker volume has been mapped with an accuracy better than 0.1%. This precision is crucial for physics analyses as it allows accurate measurements of charged particle track parameters near the interaction vertex.

Outside the tracker volume, the field map is calculated with the finite-element computation described in Section 3. Between the tracker and the first barrel muon station the magnetic field integral is dominated by the relatively homogeneous field inside the coil ($R < 3$ m). In this region, the accuracy of the computation is confirmed by its agreement within 0.06% with fixed Nuclear Magnetic Resonance (NMR) probes located at $R = 2.91$ m (cf. Section 5.1). An additional test of the accuracy of the field map inside the solenoid is given by the comparison of the predicted and observed bending of cosmic ray tracks between the silicon tracker and the first muon station. For this purpose, cosmic muons reconstructed with the inner tracker are extrapolated to the first muon station using the calculated field map. The residual between the measured and the extrapolated positions, Δ, is computed separately for positive and negative muons, and their charge-antisymmetric combination ($(\Delta^{\mu^+} - \Delta^{\mu^-})/2$) is used to suppress the possible effect of a residual misalignment. The result is plotted in Fig. 2. The expected effect of a 0.1% distortion of the field map in the region located between the tracker and the first muon station, relative to the field inside the tracker, is shown as a reference. We conclude that the map describes the field in this region within this accuracy.

The muon momentum and charge are mostly determined by the curvature of the reconstructed track in the tracker [5]. Only at very high transverse momentum a track fit combining hits in the tracker and in the muon system is expected to improve the resolution, due to the long additional lever arm with high magnetic field between the outer layer of the tracker and the muon system. Studies with cosmic muons show that the most critical factor in this global fit is alignment [6, 7].

A measurement of the muon momentum can also be obtained exclusively using information from the muon chambers. This "stand-alone" muon reconstruction is used in the hardware-based Level-1 muon trigger and in the first stage of the High-Level Trigger [8]. The resolution that can be obtained in this case is limited by multiple scattering, by the finite resolution of
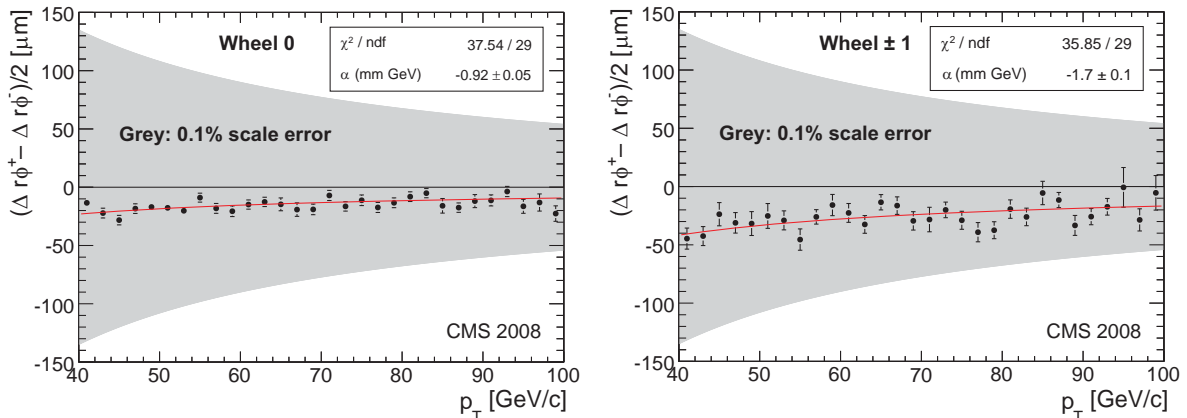
Figure 2: Residual distances, in the bending plane, between the extrapolation of the tracker tracks and the measurements in the first muon station, for the CRAFT cosmic muon data set, as a function of the transverse momentum. Left: wheel 0. Right: wheels ± 1. The shaded area shows the expected effect of a 0.1% distortion of the field map in the region between the inner tracker and the coil. The solid line represents a fit to the function α / p_T.

the muon chambers, and by their alignment. Ideally, the magnetic field map should be known with sufficient accuracy so that a possible biasing effect on the momentum scale is small compared to the resolution of the momentum measurement. While a systematic momentum bias is an uncertainty of a fundamentally different nature than the detector resolution, this requirement ensures that the efficiency of matching tracker tracks to muon hits for identification and reconstruction purposes is not reduced, and that the sharpness of trigger turn-on curves is not affected by spatially inhomogeneous inaccuracies of the field map.

An analytical calculation was used to estimate how the fitted muon momentum is affected by the inaccuracies of the magnetic field map in the yoke [9]. The largest effects occur if only the bending power provided by the return field in the yoke is considered, without constraining the fitted muon tracks to the beamspot ("vertex constraint"). Figure 3 shows at which point the relative systematic bias on the momentum due to limited knowledge of the field is ten times smaller than the resolution of the stand-alone momentum measurement deriving from hit resolution and multiple scattering, under the assumption of perfect detector alignment. The most stringent condition on B in a single layer is found in the second layer of the return yoke, where the magnetic field systematic uncertainty is required to be below 5% at intermediate momentum. If all layers are affected by a fully correlated scaling factor, this value becomes 3%. Thus, to ensure that the systematic uncertainty due to the inaccuracy of the field map is negligible, the benchmark is set at 3% for the overall scale uncertainty and at 5% for the scale in individual plates in the barrel return yoke.

These limits are conservative, as they are obtained for the extreme case of a fit with no vertex constraint. The constrained fit profits from the lever arm and bending power between the vertex and the first layer of the muon system, improving the precision of the fit for muons originating from the interaction region and reducing the reliance on the accuracy of the field in the return yoke by one order of magnitude.
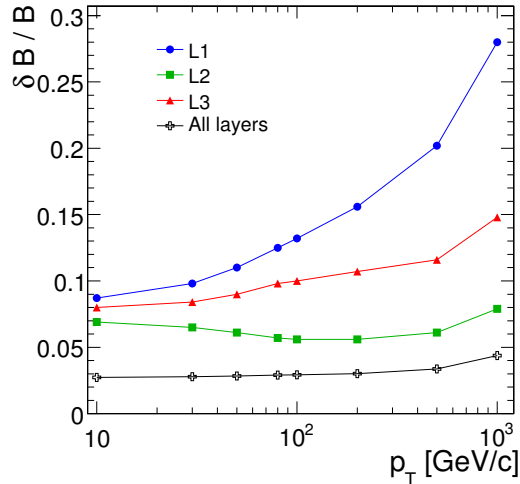
Figure 3: The systematic uncertainty in the *B* scale that corresponds to a systematic uncertainty in the determination of the muon momentum equal to one tenth of the momentum resolution, for muons reconstructed using the barrel muon spectrometer alone and without a vertex constraint. The different curves correspond to a coherent scaling of *B* in a single yoke layer, without changing the field in other layers (curves labeled "L1", "L2", "L3") and to a scaling in all layers with the same factor (curve labeled "All layers").

3   Finite-Element Model of the CMS Magnetic Field

In order to establish a map of the CMS magnetic field, the CMS solenoid and yoke were modeled using the TOSCA finite element program [10]. We summarize here the main features of this model, which is described in detail elsewhere [11].

The orientation of the CMS reference frame and the naming conventions used in this paper for the different parts of the steel yoke are shown in Fig. 1. CMS uses a right-handed coordinate system, with the origin at the nominal collision point, the x-axis pointing to the centre of the LHC, the y-axis pointing up (perpendicular to the LHC plane), and the z-axis along the anticlockwise-beam direction. The azimuthal angle, ϕ, is measured from the positive x-axis in the x-y plane.

The steel yoke is composed of 12 azimuthal sectors, and is therefore to a good approximation 12-fold ϕ-symmetric, except for a few features:

- the presence of radial passages in steel slabs ("chimneys") to route cryogenic and electric connections in sector 3 of wheel -1 (with a depth along z of 39 cm and 84 cm wide) and sector 4 of wheel +1 (39 cm deep and 54 cm wide);
- the presence of supporting feet in sectors 9 and 11;
- the presence of the carts supporting the endcap disks;
- the presence of a steel plate on the floor under the detector.

The entire length of CMS along the z-axis had to be modeled since the winding of the CMS solenoid is not exactly z-symmetric, affecting the field in the inner tracker region. However, due to limitations on the maximum number of nodes in the TOSCA mesh only the $x > 0$ half of the CMS detector was modeled. This choice allows an approximated map of the field in the entire detector to be obtained using the 12-fold symmetry of the yoke with a special treatment of the features described above, as will be discussed in the next section.
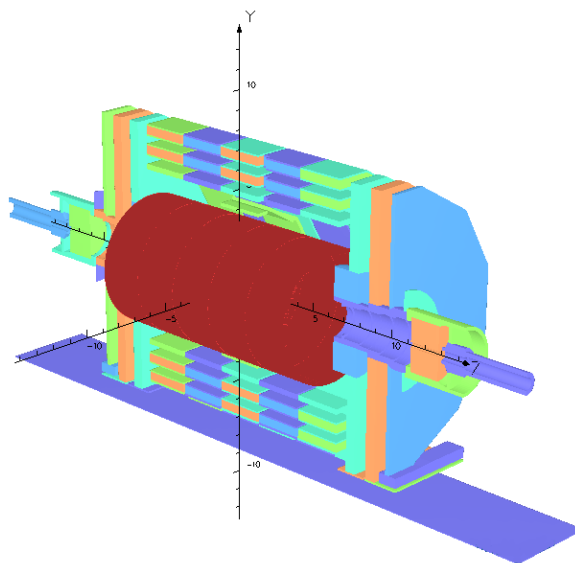
Figure 4: Representation of the magnetic elements included in the TOSCA model (underground configuration).

Two different yoke configurations have been modeled. The first ("surface model") represents the status of the CMS detector during the mapping campaign of 2006, that was performed in the surface hall. At that time, the small outermost endcap steel disk shown in Fig. 1 was not present in the negative-z endcap, and neither were any ferromagnetic parts beyond $|z| > 10.86$ m, i.e., the forward hadron calorimeters and the shielding of the LHC magnets. This configuration is used only for comparison with the 2006 measurements. The second ("underground model") represents the final setup of CMS in the experimental hall.

Figure 4 shows a representation of the model geometry. The predicted magnetic flux density on a longitudinal section of the CMS detector is shown in Fig. 5. Approximately two thirds of the magnetic flux return through the barrel yoke, half of which enters directly into the barrel without passing through the endcap disks. One third of the total flux escapes radially, returning outside the steel yoke. For this reason, particular care has to be taken in modeling boundary positions. Truly open boundaries cannot be specified with TOSCA. The simplest way to approximate open boundaries is to compute the field in a large region enclosing the solenoid and yoke. The effect of different choices for the enclosing volume on the same TOSCA model is shown in Fig. 6. A small enclosing region (e.g., $R < 13$ m) forces too much flux to return in the yoke, causing a distortion in the region instrumented with muon detectors ($4 < R < 7.4$ m). By increasing the enclosing region to $R < 26$ m, the total flux returning through the yoke is reduced by about 15%. A further increase to a region $R < 30$ m gives an additional reduction of only about 1%. The region enclosing the model cannot be enlarged indefinitely without reducing the precision of the calculation, due to the limitations in the number of mesh points in TOSCA. Except where otherwise specified, the models used in the rest of this paper are computed in the largest of the regions considered in Fig. 6. Any residual effect due to boundary positions, as well as the effect of additional magnetic material in the experimental cavern (in particular, reinforcement steel in the concrete walls, that is not included in the model) has to be estimated and calibrated out with real data, as discussed in Section 6.
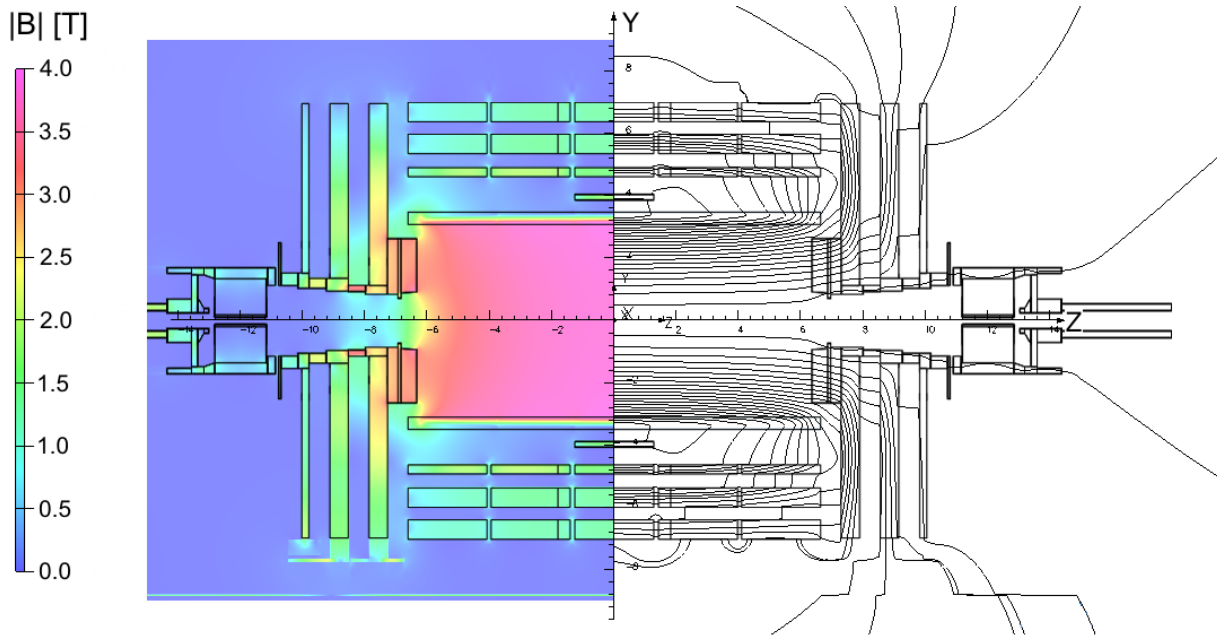
Figure 5: Value of $|B|$ (left) and field lines (right) predicted on a longitudinal section of the CMS detector, for the underground model at a central magnetic flux density of 3.8 T. Each field line represents a magnetic flux increment of 6 Wb.
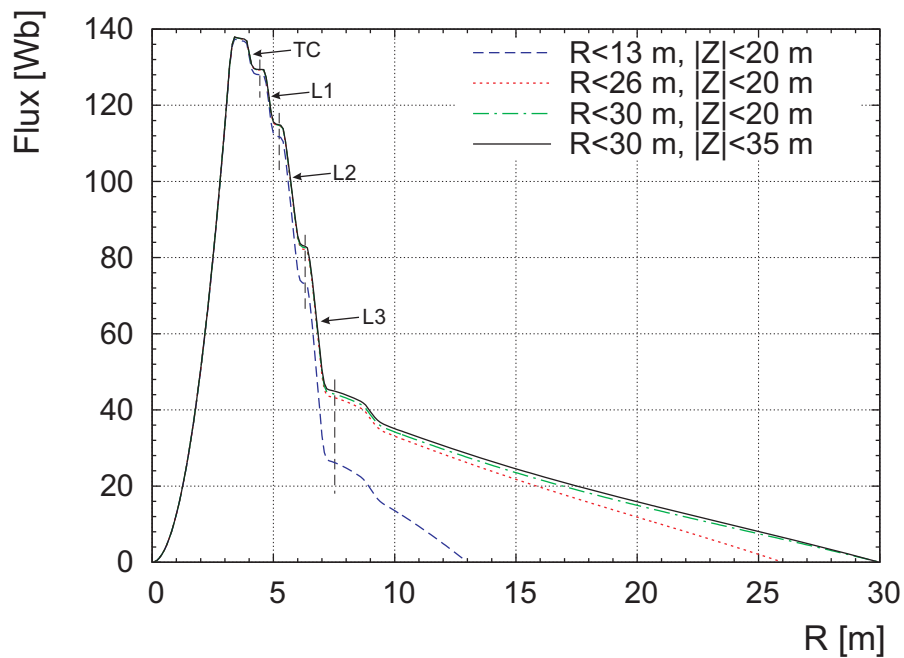
Figure 6: Magnetic flux through a disk of radius R in the transverse plane at $z = 0$ m, as predicted by the TOSCA model for the surface configuration and 4 T operating conditions, computed within different enclosing regions. The vertical dashed lines indicate the location of the four barrel muon stations.

4 The Field Map for Simulation and Reconstruction

Simulation and reconstruction of events in the CMS detector require knowledge of the magnetic field in the entire detector, both in the inner tracking region and in the complex configuration of the steel return yoke. Besides accuracy, computing efficiency of the map interface is a key requirement, as the map is accessed intensively during the on-line reconstruction in the High-Level Trigger.

An optimized interface [12] to the data obtained from the TOSCA computation described in the previous section was developed in the framework of the standard CMS software, to be used for Monte Carlo simulation, High-Level Trigger, and offline reconstruction.

The map is implemented using a dedicated, volume-based geometry model. The detector is subdivided in volumes, which correspond to the volumes used in TOSCA to define the magnetic properties of the different materials. Their boundaries correspond to the field discontinuities due to changes in the magnetic permeability of different materials. The field within each volume is therefore continuous, allowing track extrapolation algorithms to optimize the step size. Volumes are organized in a hierarchical structure optimized for fast global search. In addition, caching and navigation techniques allow simulation and track extrapolation algorithms to minimize the number of global volume searches.

Within each volume, the field is obtained either by interpolation of the values computed with TOSCA on a three-dimensional grid adapted to the volume shape so that it is regular in an appropriate coordinate system, or by parameterizations of the TOSCA computation when available. Although the different volumes constituting the CMS detector can use specific grid tables, symmetries can be exploited to reduce the memory footprint of the map. In particular, a compact field map of the entire CMS detector has been produced exploiting the 12-fold ϕ-symmetry of the yoke, with special treatment of the main ϕ-asymmetric features described in Section 3. For this purpose, specific grid tables are used for the three barrel steel layers in the sectors containing chimneys (S3, S4). Specific tables are also used in the bottom sectors (S9, S10, S11) of the outermost barrel steel layer and of the endcap disks, that are influenced by the presence of the feet and carts. The field in all other sectors is obtained with appropriate rotations from the grid tables of sector 1, which is chosen as it is well separated from the ϕ-asymmetric features of the yoke. This choice represents a compromise between accuracy, memory footprint, and complexity of the map.

5 Direct Field Measurements

Detailed measurements of the magnetic field using various sensors were performed in 2006 in the surface hall. These results have been complemented with new measurements in the cavern during the CRAFT campaign. In this section, the measured values are compared with the latest TOSCA computations.

5.1 Measurements within the tracker volume

The field inside the coil was measured in the surface hall, before lowering CMS into the experimental cavern and before the installation of the tracker and of the electromagnetic calorimeter. A pneumo-mechanical field mapper was used to scan a cylinder of radius 1.724 m and length 7 m, providing precise measurements for 33 840 space points. A detailed description of the device and of the results is given in Ref. [13].

The field has been measured at several values of B_0, the central magnetic flux density: 2, 3,

Table 1: Comparison of the magnetic flux density measured by fixed NMR probes inside the solenoid on the surface and underground, for different coil currents. Each measurement is performed with one single probe, although different probes are used in different operation ranges. Probes are located at $R = 2.91$ m, $z = -0.01$ m. The relative precision of the measurements is better than 5×10^{-5}. The prediction of the underground TOSCA model at 18 160 A ($B_0 = 3.8$ T) for the location of the probe at $\phi = 44.9°$, where the relative variation of $|B|$ is expected to be smaller than 3×10^{-4} for a displacement of 1 cm, is 3.9181 T.

Current [A]	Probe ϕ	Surface [T]	Underground [T]	Δ [T]
7 000	$-135.1°$	1.5218	1.5224	-0.0006
9 500	$-135.1°$	2.0616	2.0628	-0.0012
18 160	$44.9°$	3.9176	3.9206	-0.0030

3.5, 3.8 and 4 T. Comparison with the TOSCA model shows excellent agreement with the measurements at $B_0 = 4$ T, with a discrepancy smaller than 5 mT. The model reproduces a small $z-$asymmetry of the magnetic flux density caused by one missing turn of the coil out of the 2180 designed turns, which was discovered during the field mapping campaign.

For optimal representation of these data, a ϕ-symmetric parametrization has been implemented using an expansion of the magnetic scalar potential over spherical harmonics represented in a cylindrical coordinate system, satisfying the Laplace equation [14]. The expansion coefficients fitted from the measured field values resulted in a map of the field in the volume comprising the inner tracker that agrees with the ϕ-averaged measurements within 0.2 mT. This fit includes a refinement of the estimated gains and offsets of the Hall probes, with the overall scale set by NMR probe measurements, confirming and further improving the initial 5×10^{-4} accuracy of the calibration. This analysis confirms the excellent quality of the field mapper measurements. The parametrization is available for processing as an option for applications that require the highest possible accuracy and for studies of systematic uncertainties related to the magnetic field. The default setting for simulation, tracking, and High-Level Trigger is to use the standard map based on TOSCA (cf. Section 3), which is sufficiently precise and computationally less demanding.

Simulation studies have shown that the different magnetic environment inside the experimental cavern has effects on the overall scale of the field in the yoke. However, the effect on the field inside the solenoid is negligible. This has been confirmed by comparing measurements with fixed NMR probes installed near the inner wall of the superconducting coil cryostat, taken at the same coil current on surface and underground (see Table 1). At the time of the underground measurements, the inner tracker and the electromagnetic calorimeter were installed inside the solenoid. It can be concluded that the measurements of the field on the surface are applicable also for operation in the cavern.

In conclusion, the field in the CMS inner tracker region is known to better than 0.1%, and the agreement of the TOSCA model with the measurements at $B_0 = 4$ T is better than 5 mT everywhere in the mapped region. Moreover, hit position residuals for tracks extrapolated from the tracker to the first muon station (see Fig. 2) validate the predicted field integral outside the mapped region. This allows the field in the inner tracker region to be used as a reference to probe the field in the yoke with cosmic tracks, as will be discussed in Section 6.

5.2   Measurements of the field inside the yoke

A measurement of the average magnetic flux density inside the steel blocks of the CMS yoke was performed in the surface hall in 2006, with a system of 22 flux loops [11] made of 315–495 turns wound around the steel plates of sector 10 in the barrel wheels W0, W-1, and W-2, and in the endcap disks D-1 and D-2, as shown in Fig. 7. The areas enclosed in the flux loops vary
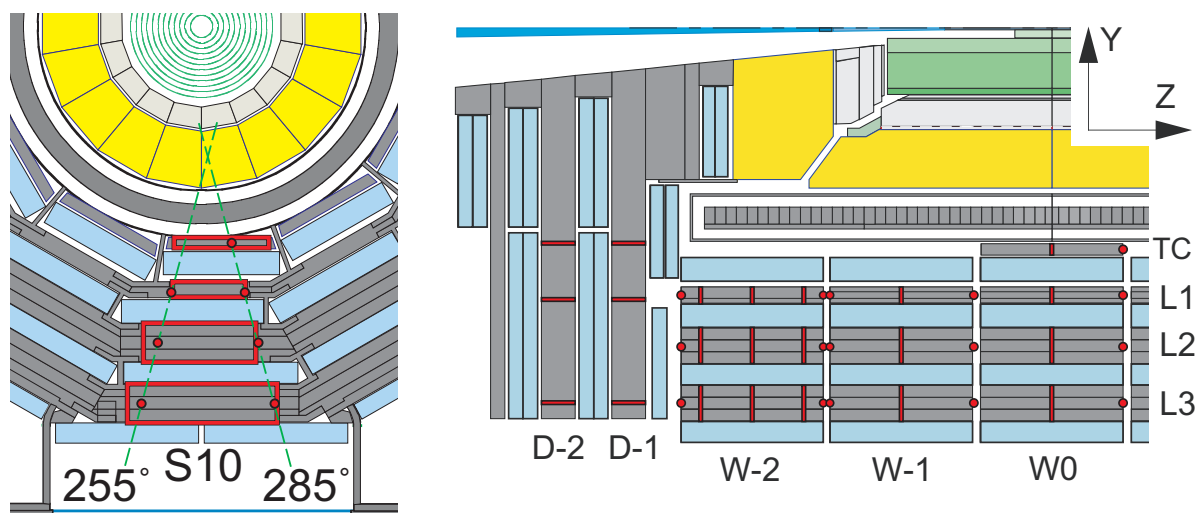

Figure 7: Location of flux loops (lines) and Hall probes (circles), projected on transverse (left) and longitudinal (right) sections of CMS.

from 0.3 to 1.7 m^2 in the barrel wheels and from 0.5 to 1.2 m^2 in the endcap disks. During a "fast" discharge of the coil (190 s time constant) from the full current to zero, voltages with amplitudes up to 3–4.5 V were induced in the loops. The integration of the measured voltages allows the average magnetic flux density in the steel blocks to be derived. At a central magnetic flux density of 4 T, the measured magnetic flux densities in the barrel wheels vary from 0.6 to 2.1 T. In the endcap disks, the measurements vary from 1.4 to 2.3 T.

The measured magnetic flux density is reduced by the residual magnetization of the steel after the fast discharge. Half of the maximum remanent field, that in the different plates varies between 54 and 85 mT depending on the steel type, is taken as an uncertainty on the measurement. The precision of the voltage measurements results in an additional uncertainty of 1.5% on the measured flux. The total uncertainty is therefore estimated to be 2% to 7% in the different loops. A comparison with the prediction of the TOSCA surface model shows that the average ratio of measured over calculated values is 0.97 in the barrel, with a standard deviation of 0.07, and 0.93 in the endcap, with a standard deviation of 0.04. For some of the measurements, large discrepancies were found (reaching 22% in the barrel and 14% in the endcaps). The current understanding of the measurements, and in particular of the actual remanent magnetization in each yoke plate, is not sufficient to use them to constrain the field map to a precision of the order of 3–5%, as required for physics analysis. More precise measurements of the magnetic flux density within the steel plates, also in sectors other than S10, are possible using reconstructed tracks from cosmic rays, as discussed in Section 6. With cosmic rays detected in the underground experimental hall, it is also possible to observe and correct for effects due to the magnetic environment of the cavern; this is not possible with the available flux loop measurements, which were performed in the surface hall.

An additional measurement of the magnetic flux density in the yoke is provided by a system

Table 2: Hall probe measurements in the underground cavern at a central magnetic flux density $B_0 = 3.8$ T, compared with the values predicted by TOSCA for the same locations. Sensors are labeled according to the steel block they are located close to (cf. Fig. 1) and their ϕ, z position.

			$\phi = 285°$			$\phi = 255°$		
		z [m]	Data [T]	Calc [T]	Data/Calc	Data [T]	Calc [T]	Data/Calc
TC	W0	1.273	−0.39	−0.37	1.06			
	W0	1.273	−0.96	−0.97	0.99	−0.95	−0.97	0.98
	W-1	−1.418	−1.02	−0.97	1.06	−0.96	−0.97	0.99
L1	W-1	−3.964	−1.13	−1.12	1.00	−1.13	−1.13	1.01
	W-2	−4.079	−1.14	−1.13	1.02	−1.16	−1.13	1.02
	W-2	−6.625	−0.26	−0.31	0.82	−0.28	−0.33	0.87
	W0	1.273	−0.89	−0.95	0.94	−0.89	−0.95	0.94
	W-1	−1.418	−0.90	−0.96	0.93	−0.90	−0.96	0.94
L2	W-1	−3.964	−0.87	−0.90	0.96	−0.87	−0.90	0.96
	W-2	−4.079	−0.87	−0.90	0.96	−0.86	−0.90	0.96
	W-2	−6.625	−0.34	−0.41	0.84	−0.34	−0.41	0.84
	W0	1.273	−0.82	−0.88	0.93	−0.82	−0.88	0.93
	W-1	−1.418	−0.82	−0.89	0.92	−0.82	−0.89	0.92
L3	W-1	−3.964	−0.75	−0.78	0.96	−0.76	−0.78	0.96
	W-2	−4.079	−0.75	−0.78	0.96	−0.76	−0.78	0.96
	W-2	−6.625	−0.37	−0.49	0.76			

of Hall probes mounted between the steel blocks at selected places. These probes provide continuous monitoring and are important to verify the long-term stability of the field. The probes are mounted close to the steel blocks, but the local magnetic flux density can only be measured in the air, and therefore it is difficult to use these measurement to constrain the field map within the yoke plates. However, they can indicate overall distortions of the model, if any.

As an example, a set of measured values at a central magnetic flux density of 3.8 T is presented in Table 2 for sensors in the barrel wheels at $\phi = 255°$ and $285°$. As shown in Fig. 7, barrel sensors are located close to the front face of steel blocks, in the gap between two neighboring wheels. In these gaps, the field is mostly axial and the magnetic flux density is about two-thirds of the flux density in the center of the steel plate.

The Hall probes used in Table 2 were calibrated at 1.4 T, with a precision better than 0.1%. The observed deviations can be related to the modeling of the gaps and of local features or inhomogeneities of the steel block at the place where the probes are mounted. To highlight a possible overall distortion of the model, the ratio of the measured and calculated field has been averaged for all probes located in the same gap. Results are shown in Table 3. In the second and third yoke layers of the barrel, the data indicate a lower field than predicted by the TOSCA calculation. A larger discrepancy is present in the gap between the barrel and the endcap.

In the endcaps, Hall probes are installed between disks, to monitor the field close to the steel surface. In this region, the field is small (with measured values in the range between 0.01 and 0.34 T) and almost axial, so the measured values cannot be easily related to the field in the steel disks, which is large and radial (cf. Fig. 5).

Table 3: Ratio of the measured and calculated values of Table 2, averaged for the probes located in the same gap (or in z-symmetric gaps in case of W0/W-1). The largest observed difference between any two of the values that are averaged together is 0.08.

	Gap W0/W±1	Gap W-1/W-2	Gap W-2/endcap
L1	1.01	1.01	0.84
L2	0.94	0.96	0.84
L3	0.92	0.96	0.76

6 Measurements with Cosmic Ray Tracks

About 3% of the muon tracks collected during CRAFT cross the acceptance of the inner tracker. This sample can be used to verify the accuracy of the magnetic field map in the yoke using the information provided by the muon chambers, and taking the precise measurement of the track momentum in the inner tracker as a reference. This section describes a method to obtain average correction factors for the scale of the field map in each plate of the CMS barrel yoke.

6.1 The analysis method

In the barrel yoke, four stations of Drift Tube (DT) chambers are interleaved with the three steel yoke layers, as shown in Fig. 1. Each DT chamber can measure the direction of the track in the transverse plane (ϕ) with a resolution of about 1.8 mrad [15] based on eight measurement planes. The track deflection in the transverse plane between two consecutive stations, i and $i + 1$, is an ideal quantity to probe the field in the yoke plates, as it is directly related to the integral of the field along the track path:

$$(\phi_{i+1} - \phi_i)p_T = -0.3\, q \int_i^{i+1} \vec{u}_\phi \cdot \vec{B} \times \vec{dl} \tag{1}$$

where q is the muon charge, p_T is the muon transverse momentum in units of GeV/c, B is expressed in Tesla, and l in meters.

The transverse bending is dominated by the axial component of the field, B_z. The azimuthal component of the field, B_ϕ, is small given the cylindrical symmetry of the barrel yoke, and does not contribute to the bending in the transverse plane. Although the radial component, B_r, contributes to Eq. (1), its effect is small and can be neglected, both because $B_r \ll B_z$ in the barrel steel plates given the geometry of the yoke (cf. Fig. 5), and because tracks selected in this analysis have small angles with respect to the radial direction. Systematic effects due to this approximation are discussed in Section 6.3.

In order to relate the path integral in Eq. (1) to the average field inside the yoke plate, the stray field in the short path between the chambers and the steel plate can be neglected, and the track path length in the transverse plane can be approximated with the thickness L of the steel plate. With this approximation:

$$\int_i^{i+1} \vec{u}_\phi \cdot \vec{B} \times \vec{dl} \simeq \langle B_z \rangle L \tag{2}$$

where $\langle B_z \rangle$ is effectively averaged along the trajectory of the particle crossing the layer between stations i and $i + 1$.

The goal of the study presented here is not to obtain directly the value of $\langle B_z \rangle$ from Eq. (2), but to compare it with the same quantity predicted by the magnetic field map, to highlight and

possibly correct for average discrepancies. For this purpose, track parameters reconstructed in the CMS inner tracking system are extrapolated to the muon spectrometer, where they are compared with the measurements of the muon chambers, for each muon separately. The extrapolation of track parameters and of their error matrices is performed taking into account multiple scattering and energy loss. These were tuned to reproduce statistically the results of the detailed GEANT4 simulation of CMS. The simulation of the energy loss in the material between the tracker and the muon system, amounting to about 3 GeV, is correct to within an accuracy of 0.2 GeV, according to comparisons with measurements [9].

The magnetic field map is used both for the measurement of the track momentum in the inner tracker and to predict the track bending in the extrapolation. Given that the accuracy of the magnetic field map in the region inside the solenoid is good, the momentum measured by the inner tracker can be taken as reference. A systematic difference between the track direction measured in the DT chambers and the direction of the extrapolated tracks can therefore be attributed to a difference between the true magnetic field integral along the particle path and the corresponding integral in the field map used for the extrapolation. Using Eq. (1), it is possible to measure the bias of the field integral in the steel layer placed between two consecutive DT stations:

$$\Delta = [(\phi_{i+1}^{\mathrm{prop}} - \phi_{i+1}^{\mathrm{data}}) - (\phi_i^{\mathrm{prop}} - \phi_i^{\mathrm{data}})] \cdot p_T \propto \int_i^{i+1} \vec{u}_\phi \cdot \vec{B}^{\mathrm{map}} \times d\vec{l} - \int_i^{i+1} \vec{u}_\phi \cdot \vec{B}^{\mathrm{true}} \times d\vec{l}, \quad (3)$$

where ϕ_i^{prop} and ϕ_i^{data} are the bending angles at the ith DT station for the propagated track and for the track segment reconstructed in the DT chamber, respectively; p_T is the muon momentum, assumed constant along the path between the two stations and obtained from the extrapolation of the inner tracker track to the middle plane between the stations, accounting for energy loss; and $\int_i^{i+1} \vec{u}_\phi \cdot \vec{B}^{\mathrm{true}} \times d\vec{l}$ and $\int_i^{i+1} \vec{u}_\phi \cdot \vec{B}^{\mathrm{map}} \times d\vec{l}$ are the true field path integral between the ith and the $i+1^{th}$ DT station and the one estimated using the field map, respectively.

The bending angles measured are potentially affected by residual misalignment. However, misalignment affects the measured angles of positive and negative muons in the same direction, while a distortion of the field map has an opposite effect on the propagated direction of tracks of opposite charge. The charge-antisymmetric combination of the mean values of the distributions of Δ for positive and negative muons crossing a given sector, in the form $(\langle\Delta\rangle_{\mu^+} - \langle\Delta\rangle_{\mu^-})/2$, is not influenced by the misalignment effects, under the assumption that positive and negative muons have the same momentum spectrum.

Equation (2) can be used to relate the right side of Eq. (3) with the average flux density in the yoke plate. The systematic uncertainties deriving from the assumptions used in writing these two expressions can be suppressed normalizing Eq. (3) to the bending expected from the field map:

$$\frac{[(\phi_{i+1}^{\mathrm{prop}} - \phi_{i+1}^{\mathrm{data}}) - (\phi_i^{\mathrm{prop}} - \phi_i^{\mathrm{data}})] \cdot p_T}{(\phi_{i+1}^{\mathrm{prop}} - \phi_i^{\mathrm{prop}}) \cdot p_T} = \frac{\langle B_z^{\mathrm{map}}\rangle - \langle B_z^{\mathrm{true}}\rangle}{\langle B_z^{\mathrm{map}}\rangle}\bigg|_{i+1/i}. \quad (4)$$

Charge-antisymmetric combinations are computed separately for the numerator and the denominator of the expression on the left side. Each yoke plate is treated separately. The expression on the right side represents the relative discrepancy of the flux density averaged over a single yoke plate.

The ratio $\langle B_z^{\mathrm{true}}\rangle / \langle B_z^{\mathrm{map}}\rangle$ is computed using Eq. (4). It can be interpreted as the corrective scaling factor that has to be applied to the $\vec{B}$ vector given by the magnetic field map, in each point

Table 4: Scaling factors for the field map described in Section 4, averaged between opposite wheels. Reported errors represent the statistical uncertainty only.

	wheels ± 2	wheels ± 1	wheel 0
L1	0.99 ± 0.04	1.004 ± 0.004	1.005 ± 0.005
L2	0.96 ± 0.02	0.958 ± 0.003	0.953 ± 0.003
L3	0.92 ± 0.08	0.924 ± 0.003	0.906 ± 0.003

within the considered steel yoke plate, in order to obtain the best estimate of B_z^{true} that reproduces the measured track bending as observed in that plate.

6.2 Results in the barrel yoke

This technique was applied on the sample of cosmic rays collected during the CRAFT campaign [4]. Only runs with stable magnet conditions at a central magnetic flux density of 3.8 T were selected. The inner tracker and the DT chambers were aligned using cosmic muon tracks, survey measurements and optical systems [7, 16, 17]. DT segments reconstructed in the transverse plane ($R - \phi$) were required to include at least seven hits out of the eight available measurement planes in a chamber. Tracks to be used in the analysis were required to be reconstructed by the inner tracker with at least 10 hits and to have a momentum within $15 < p_T < 100 \,\mathrm{GeV}/c$. In addition, the extrapolated track path was required to pass through all four DT stations in the same sector and wheel. About one million tracks survive these pre-selection requirements.

For the computation of scaling factors to be used to calibrate the field map, additional selection criteria were applied in addition to the pre-selection requirements, to select data of the best quality. Only runs of certified good quality by the Data Quality Monitoring system for both the Drift Tube system and the inner tracker were used, and tracks were selected with a transverse impact parameter with respect to the centre of CMS, $|d_0|$, less than 0.4 m and a longitudinal impact parameter, $|d_z|$, less than 1 m. This tighter selection retains about 0.6 million events. The reduction in the size of the event sample is mostly due to the increased pointing requirement and, therefore, is especially severe (about a factor 5) in wheels ± 2. Scaling factors were computed using the field map described in Section 4. Results for all sectors of a given layer and wheel, as well as results for opposite wheels, were found to be compatible within statistical uncertainties, as expected given that the main ϕ- and z-asymmetric features are described in this map; they have, therefore, been averaged. The resulting factors, listed in Table 4, are adopted as correction factors for the magnetic flux density in the map used in the CMS software for reconstruction and simulation.

The values measured with tracks show the same trend as observed with Hall probe measurements in the barrel (first two columns of Table 3), although a direct numerical comparison is not possible, as the Hall probe measurements are performed in the gaps between wheels while the tracks probe the field inside the steel plates.

To verify the consistency of the method, the scaling factors were recomputed using the corrected map, for events passing the pre-selection criteria only. The resulting factors, shown in Fig. 8, are compatible with unity within statistical uncertainties. In order to search for possible biases they were averaged, grouping sectors in different ways. The results are listed in Table 5. No bias is found to significantly exceed the statistical uncertainties. In particular, upper and lower sectors agree well within statistical uncertainties indicating that potential systematic biases due to the material budget description are under control at the sub-percent level. A
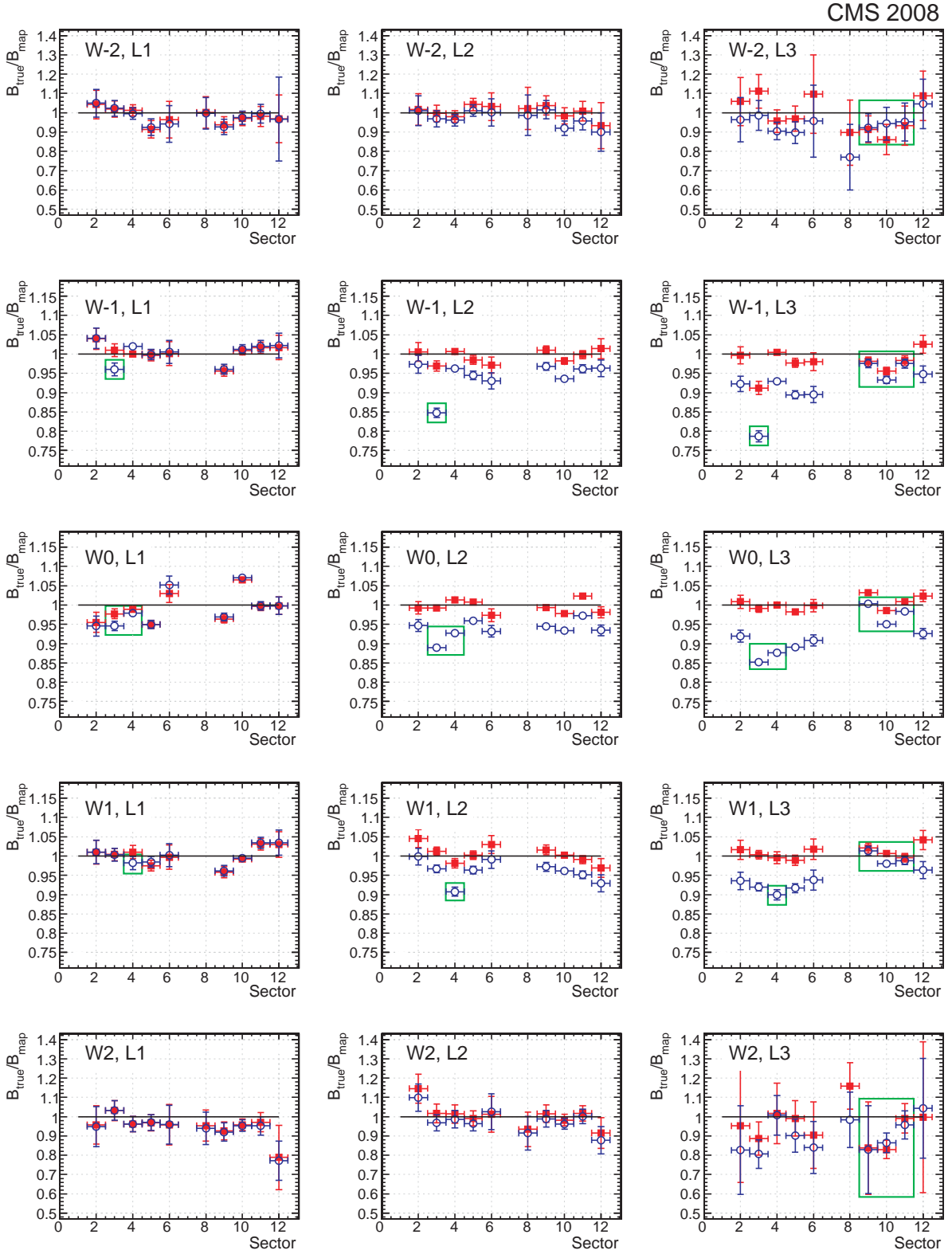
Figure 8: Solid squares: average values of $\langle B_z^{\mathrm{true}} \rangle / \langle B_z^{\mathrm{map}} \rangle$, after the correction factors of Table 4 are applied. Open circles: Scaling factors obtained using a 12-fold ϕ-symmetric map, with no correction and no special treatment of the ϕ-asymmetric features described in Section 4. The sectors affected by these features have been highlighted with open boxes. Data points are not reported in sectors where the available event samples are too small (in particular, sectors around $y = 0$, where the chambers are installed vertically). Error bars only include the statistical uncertainty.

Table 5: Consistency check: average values of $\langle B_z^{\text{true}} \rangle / \langle B_z^{\text{map}} \rangle$, after the correction factors of Table 4 are applied. Errors represent the statistical uncertainty of the method only.

All sectors	0.998 ± 0.001
All top sectors	0.997 ± 0.002
All bottom sectors	0.999 ± 0.002
All $x > 0$ sectors	1.002 ± 0.003
All $x < 0$ sectors	0.995 ± 0.003
All sectors (only L1)	0.997 ± 0.002
All sectors (only L2)	1.000 ± 0.002
All sectors (only L3)	0.997 ± 0.002
All sectors in wheel 0	1.000 ± 0.002
All sectors in wheels ± 1	0.998 ± 0.001
All sectors in wheels ± 2	0.984 ± 0.007

discrepancy in the energy loss estimation should be visible as an opposite bias in the top and bottom scaling factors, given the propagation direction of the cosmic muons. The 2.3 σ difference in the average for all sectors in wheels ± 2 is due to the fact that the correction factors of Table 4 were computed with a significantly smaller sample because of the tighter selection, an effect particularly important in these wheels.

To highlight the effect of the handling of the specific ϕ-asymmetric yoke features described in Section 4, the analysis was repeated on a ϕ-symmetric map with no special sector handling and no correction factors. The results, for all events passing the pre-selection criteria, are shown in Fig. 8, separately for each sector and yoke layer. On top of the already observed overall scale bias in the different layers, the effect of the chimneys is visible in sector 3 in wheel -1, sector 3–4 in wheel 0, and sector 4 in wheel $+1$. Also the effect of the feet is visible in sectors 9, 10 and 11 of layer 3, where scaling factors are higher than in the neighboring sectors. In these locations, the true field integral is expected to be higher because of the extra steel due to the feet supporting the yoke (see Fig. 1). The handling of these features in the default map reduces their effect.

The analysis was cross-checked against a simulated cosmic muon sample. Cosmic muons were simulated with a Monte Carlo generator (CMSCGEN [18]), interfaced to the full GEANT simulation of the detector. Only cosmic muons with a momentum of at least 10 GeV/c at the entrance point in CMS were simulated. A realistic misalignment of the silicon tracker and of the muon chambers corresponding to the CRAFT data was applied to the reconstructed tracks and muon segments, and the same pre-selection as used for the data was applied. Since in the simulation B_z^{true} is identical to B_z^{map} in every point in CMS by definition, this study provides a powerful check of the calibration of the method. The measured scaling factors have been verified to be compatible with unity in all sectors. The overall result shows that in the simulation, without further calibration, the method provides a scaling factor accurate to better than a percent ($-0.7 \pm 0.4\%$). No evidence is seen of any dependence versus radius (L1 – L3), versus z (wheel 0 – wheel 2), or propagation direction (bottom versus top).

6.3 Systematic Uncertainties

As shown in the previous section, the available data sample of cosmic muons can be used to constrain the scale of the magnetic field with a statistical accuracy better than a percent in most of the barrel return yoke. Possible systematic uncertainties in the method are discussed in this

section. While the magnetic field map only provides a value of the B vector in every point, without an associated uncertainty, this information can be used in physics measurements to derive systematic uncertainties due to the mismodeling of the magnetic field, by studying the effect of an appropriately distorted field map.

A first systematic effect can arise from the assumption that a good representation of the true magnetic field can be obtained by applying the ratio $\langle B_z^{\text{true}} \rangle / \langle B_z^{\text{map}} \rangle$ measured from Eq. (4) as a corrective scaling factor to the $\vec{B}$ vector in the field map, in each point within the corresponding steel yoke plate. A single scaling factor per steel block can correct for the average magnetic field discrepancy, but not for its local variations within the block.

To quantify the possible magnitude of these variations, it is useful to have a model of (realistic) distortions, somewhat larger than the observed ones. The TOSCA model computed using the smallest enclosing model boundaries of those described in Fig. 6 ($R < 13$ m and $z < 20$ m) is used for this purpose. Reducing the volume boundaries forces more magnetic flux to return through the yoke, and therefore provides a "physical" distortion of the magnetic field map, still satisfying Maxwell's equations while providing natural variations in all B components (unlike a single scaling factor for all field components in a given region). The magnitude of the distortion in this model is arbitrary. Given that discrepancies with respect to the default model in the barrel yoke layers are at least twice as large as the actual measured discrepancies reported in Table 4, all systematic effects that are estimated from the comparison of this model with the default one are scaled down by a factor 2.

The ratio between the value of B predicted by the standard and distorted models is computed as a function of the position inside a plate. Its variation within the plate, that is found as expected to be much smaller than the variation of B itself, represents the variation that the scaling factor would have in the different regions of the plate. Since the method described in Section 6.1 averages the scaling factor in the plate, and over a region that covers a limited z range due to track selection criteria, a systematic uncertainty is estimated as half of the maximum observed variation between any two points within the plate. This correspond to $\pm 0.5\%$ in all layers and wheels, except for layer 1 of wheels ± 1 and ± 2, where the variations are $\pm 2.5\%$ and $\pm 2\%$, respectively. This is the region of the yoke where the field is the highest and closest to saturation, giving rise to deviations from linear scaling. This systematic uncertainty could be reduced by deriving scaling factors for smaller regions in z and ϕ, at the cost of larger statistical uncertainties.

Other systematic effects can arise from the assumptions, discussed in Section 6.1, used to derive the average scaling factors:

- Effect of B_r. The radial component of the field is neglected in the analysis, although it can affect the measured bending. This component is negligible in most of the barrel yoke, except in the two inner steel layers of wheel ± 2, where it reaches 0.4 T. The presence of a B_r component affects both the real muon bending and the track extrapolation, so to first order its effect cancels in their comparison and in the ratio of Eq. (4). A bias on the measured scaling factor is expected only if the ratio $B_r^{\text{true}} / B_r^{\text{map}}$ differs from the ratio $B_z^{\text{true}} / B_z^{\text{map}}$. The distorted field map described above was used as a model of a physical distortion of both components. The resulting bias on the measured scaling factor is estimated to be 0.5% in L1 and L2 of W± 2, and negligible elsewhere.

- Assumption of ϕ and z-symmetry in averaging scaling factors. As described in Section 4, the current field map is implemented assuming 12-fold ϕ-symmetry of the

yoke, with a specific handling of sectors affected by the presence of chimneys, feet and carts. As a result of the specific description of these special sectors, the measured scaling factors for all sectors in each layer and wheel, as well as in opposite wheels, are compatible and can be averaged. However, residual differences can be present also among the sectors where symmetry is assumed to hold. Differences of up to $\pm 1\%$ in the field integral for a path traversing radially these yoke layers are predicted by the TOSCA model. A systematic uncertainty of $\pm 1\%$ due to the assumption of symmetries in the averaging of the scaling factors is therefore estimated.

Finally, the main input to the analysis is the muon segment angle measured in each DT station, which can be affected by the imperfect knowledge of the internal geometry of the chambers. Each chamber is composed of three groups of layers of drift cells, called superlayers, that are superimposed [1]. The assembly procedure can give an uncertainty in the distances between the superlayers of about 1 mm [5] for a typical distance of approximately 25 cm. The corrective scaling factors, $B_z^{\text{true}}/B_z^{\text{map}}$, are evaluated from the difference between the angles measured in consecutive stations and are, hence, particularly sensitive to a correct description of their different internal geometries. An uncertainty of 2% on the scaling factors has been computed assuming an unaccounted difference of 1 mm in the internal distance between the two superlayers composing the chambers of two consecutive stations. This effect is expected to vary from sector to sector as it is the result of the interplay between the distribution of incident angles in a given sector and the individual chamber geometry.

The statistical and systematic uncertainties on the measured scaling factors are summarized in Table 6.

Table 6: Summary of statistical and systematic uncertainties on the measured scaling factors. The columns report the statistical uncertainty of the measurement and the estimated systematic uncertainties due to: the variation of the actual discrepancies within each plate; the neglected radial component of the magnetic field; the assumption of ϕ and z-symmetry in averaging scaling factors; and the internal geometry of the DT chambers. The last column gives the total uncertainty (sum in quadrature of the partial terms).

Uncertainty (%)	Statistical	Local variation	B_r	Symmetry	Geometry	Total
W0, L1	0.5	0.5	-	1.0	2.0	2.3
W0, L2	0.3	0.5	-	1.0	2.0	2.3
W0, L3	0.3	0.5	-	1.0	2.0	2.3
W$\pm$1, L1	0.4	2.5	-	1.0	2.0	3.8
W$\pm$1, L2	0.3	0.5	-	1.0	2.0	2.3
W$\pm$1, L3	0.3	0.5	-	1.0	2.0	2.3
W$\pm$2, L1	3.8	2.0	0.5	1.0	2.0	4.8
W$\pm$2, L2	2.4	0.5	0.5	1.0	2.0	3.4
W$\pm$2, L3	7.7	0.5	-	1.0	2.0	8.0

The scaling factors measured in the present study are insensitive to the radial distribution of the field map discrepancy inside steel blocks; they simply correct the integral of B along the path. For example, the two outermost barrel steel layers consist of a sandwich of three steel plates with different magnetic properties; the actual discrepancy of the map may be different in each one. While such radial variations of the discrepancy with respect to the average can affect the predicted position of a muon after traversing the plate, they have no effect on the bending angle.

The measured average discrepancies do not exclude larger localized discrepancies. Local deviations are, however, constrained by the continuity of the magnetic flux.

7   Conclusions

The magnetic flux density in the steel plates of the CMS barrel return yoke was measured precisely using cosmic ray muons, leading to a fundamental improvement in the understanding of the CMS magnetic field. The results are consistent with the indication of measurements with Hall probes installed in the gaps between wheels. Based on these measurements, an improved map of the CMS magnetic field for the central magnetic flux density planned for the first years of physics operation ($B_0 = 3.8$ T) has been provided for simulation, High-Level Trigger, and track reconstruction. In the CMS yoke, the new map is estimated to be accurate to better than 3% in the steel of the three central barrel wheels, and to about 8% in the steel of the two outermost barrel wheels, satisfying the accuracy required for physics analysis and muon triggering in CMS.

Acknowledgments

References

[1] **CMS** Collaboration, "The CMS experiment at the CERN LHC", *JINST* **3** (2008) S08004.
`doi:10.1088/1748-0221/3/08/S08004`.

[2] L. Evans and P. Bryant (eds.), "LHC machine", *JINST* **3** (2008) S08001.
`doi:10.1088/1748-0221/3/08/S08001`.

[3] **CMS** Collaboration, "The Magnet Project Technical Design Report", *CERN/LHCC* **97-010** (1997).

[4] **CMS** Collaboration, "Commissioning of the CMS Experiment and the Cosmic Run at Four Tesla", *submitted to JINST* (2009).

[5] **CMS** Collaboration, "CMS Physics TDR: Volume I, Detector Performance and Software", *CERN/LHCC* **2006-001** (2006).

[6] **CMS** Collaboration, "Studies of CMS Muon Reconstruction Performance with Cosmic Rays", *submitted to JINST* (2009).

[7] **CMS** Collaboration, "Alignment of the CMS Muon System with Cosmic Ray and Beam-Halo Tracks", *submitted to JINST* (2009).

[8] **CMS** Collaboration, "The CMS High-Level trigger", *Eur. Phys. J.* **C46** (2006) 605–667. `doi:10.1140/epjc/s2006-02495-8`.

[9] L. Bianchini, "Search for a Z' at the LHC and Magnetic Field Calibration in the CMS Barrel Yoke", *Master thesis* **CMS TS-2009/016** (2009).

[10] Vector Fields Ltd.. Oxford, U. K., "TOSCA/OPERA-3d Software", *www.vectorfields.com*.

[11] V.I. Klyukhin et al., "Measuring the Magnetic Field Inside the CMS Steel Yoke Elements", *Nuclear Science Symposium Conference Record. NSS '08. IEEE* (2008) 2270–2273. `doi:10.1109/NSSMIC.2008.4774806`.

[12] N. Amapane et al., "Volume-Based Representation of the Magnetic Field", in *Computing in High Energy Physics and Nuclear Physics 2004, Interlaken, Switzerland, 27 Sep. - 1 Oct. 2004*, p. 310. 2005. CERN-2005-002-V-1, CMS note CR-2005/011.

[13] V.I. Klyukhin et al., "Measurement of the CMS Magnetic Field", *IEEE Transactions on Applied Superconductivity* **Vol. 18, no. 2** (2008) 395–398. `doi:10.1109/TASC.2008.921242`.

[14] V. Maroussov, "Fit to an Analytic Form of the Measured Central CMS Magnetic Field", *PhD thesis* **CMS TS-2009/018** (2008).

[15] **CMS** Collaboration, "Performance of Local Muon Reconstruction in Drift Tube Chambers from the Analysis of Cosmic Run Data", *submitted to JINST* (2009).

[16] **CMS** Collaboration, "Alignment of the CMS Silicon Tracker During Commissioning with Cosmic Ray Particles", *submitted to JINST* (2009).

[17] **CMS** Collaboration, "Aligning the CMS Muon Chambers with the Muon Alignment System during the Cosmic Run of 2008", *submitted to JINST* (2009).

[18] P. Biallass and T. Hebbeker, "Parametrization of the Cosmic Muon Flux for the Generator CMSCGEN", `arXiv:0907.5514`.

A   The CMS Collaboration

Yerevan Physics Institute, Yerevan, Armenia
S. Chatrchyan, V. Khachatryan, A.M. Sirunyan

Institut für Hochenergiephysik der OeAW, Wien, Austria
W. Adam, B. Arnold, H. Bergauer, T. Bergauer, M. Dragicevic, M. Eichberger, J. Erö, M. Friedl,
R. Frühwirth, V.M. Ghete, J. Hammer[1], S. Hänsel, M. Hoch, N. Hörmann, J. Hrubec, M. Jeitler,
G. Kasieczka, K. Kastner, M. Krammer, D. Liko, I. Magrans de Abril, I. Mikulec, F. Mittermayr,
B. Neuherz, M. Oberegger, M. Padrta, M. Pernicka, H. Rohringer, S. Schmid, R. Schöfbeck,
T. Schreiner, R. Stark, H. Steininger, J. Strauss, A. Taurok, F. Teischinger, T. Themel, D. Uhl,
P. Wagner, W. Waltenberger, G. Walzel, E. Widl, C.-E. Wulz

National Centre for Particle and High Energy Physics, Minsk, Belarus
V. Chekhovsky, O. Dvornikov, I. Emeliantchik, A. Litomin, V. Makarenko, I. Marfin,
V. Mossolov, N. Shumeiko, A. Solin, R. Stefanovitch, J. Suarez Gonzalez, A. Tikhonov

Research Institute for Nuclear Problems, Minsk, Belarus
A. Fedorov, A. Karneyeu, M. Korzhik, V. Panov, R. Zuyeuski

Research Institute of Applied Physical Problems, Minsk, Belarus
P. Kuchinsky

Universiteit Antwerpen, Antwerpen, Belgium
W. Beaumont, L. Benucci, M. Cardaci, E.A. De Wolf, E. Delmeire, D. Druzhkin, M. Hashemi,
X. Janssen, T. Maes, L. Mucibello, S. Ochesanu, R. Rougny, M. Selvaggi, H. Van Haevermaet,
P. Van Mechelen, N. Van Remortel

Vrije Universiteit Brussel, Brussel, Belgium
V. Adler, S. Beauceron, S. Blyweert, J. D'Hondt, S. De Weirdt, O. Devroede, J. Heyninck, A. Ka-
logeropoulos, J. Maes, M. Maes, M.U. Mozer, S. Tavernier, W. Van Doninck[1], P. Van Mulders,
I. Villella

Université Libre de Bruxelles, Bruxelles, Belgium
O. Bouhali, E.C. Chabert, O. Charaf, B. Clerbaux, G. De Lentdecker, V. Dero, S. Elgammal,
A.P.R. Gay, G.H. Hammad, P.E. Marage, S. Rugovac, C. Vander Velde, P. Vanlaer, J. Wickens

Ghent University, Ghent, Belgium
M. Grunewald, B. Klein, A. Marinov, D. Ryckbosch, F. Thyssen, M. Tytgat, L. Vanelderen,
P. Verwilligen

Université Catholique de Louvain, Louvain-la-Neuve, Belgium
S. Basegmez, G. Bruno, J. Caudron, C. Delaere, P. Demin, D. Favart, A. Giammanco,
G. Grégoire, V. Lemaitre, O. Militaru, S. Ovyn, K. Piotrzkowski[1], L. Quertenmont, N. Schul

Université de Mons, Mons, Belgium
N. Beliy, E. Daubie

Centro Brasileiro de Pesquisas Fisicas, Rio de Janeiro, Brazil
G.A. Alves, M.E. Pol, M.H.G. Souza

Universidade do Estado do Rio de Janeiro, Rio de Janeiro, Brazil
W. Carvalho, D. De Jesus Damiao, C. De Oliveira Martins, S. Fonseca De Souza, L. Mundim,
V. Oguri, A. Santoro, S.M. Silva Do Amaral, A. Sznajder

Instituto de Fisica Teorica, Universidade Estadual Paulista, Sao Paulo, Brazil

T.R. Fernandez Perez Tomei, M.A. Ferreira Dias, E. M. Gregores[2], S.F. Novaes

Institute for Nuclear Research and Nuclear Energy, Sofia, Bulgaria
K. Abadjiev[1], T. Anguelov, J. Damgov, N. Darmenov[1], L. Dimitrov, V. Genchev[1], P. Iaydjiev, S. Piperov, S. Stoykova, G. Sultanov, R. Trayanov, I. Vankov

University of Sofia, Sofia, Bulgaria
A. Dimitrov, M. Dyulendarova, V. Kozhuharov, L. Litov, E. Marinova, M. Mateev, B. Pavlov, P. Petkov, Z. Toteva[1]

Institute of High Energy Physics, Beijing, China
G.M. Chen, H.S. Chen, W. Guan, C.H. Jiang, D. Liang, B. Liu, X. Meng, J. Tao, J. Wang, Z. Wang, Z. Xue, Z. Zhang

State Key Lab. of Nucl. Phys. and Tech., Peking University, Beijing, China
Y. Ban, J. Cai, Y. Ge, S. Guo, Z. Hu, Y. Mao, S.J. Qian, H. Teng, B. Zhu

Universidad de Los Andes, Bogota, Colombia
C. Avila, M. Baquero Ruiz, C.A. Carrillo Montoya, A. Gomez, B. Gomez Moreno, A.A. Ocampo Rios, A.F. Osorio Oliveros, D. Reyes Romero, J.C. Sanabria

Technical University of Split, Split, Croatia
N. Godinovic, K. Lelas, R. Plestina, D. Polic, I. Puljak

University of Split, Split, Croatia
Z. Antunovic, M. Dzelalija

Institute Rudjer Boskovic, Zagreb, Croatia
V. Brigljevic, S. Duric, K. Kadija, S. Morovic

University of Cyprus, Nicosia, Cyprus
R. Fereos, M. Galanti, J. Mousa, A. Papadakis, F. Ptochos, P.A. Razis, D. Tsiakkouri, Z. Zinonos

National Institute of Chemical Physics and Biophysics, Tallinn, Estonia
A. Hektor, M. Kadastik, K. Kannike, M. Müntel, M. Raidal, L. Rebane

Helsinki Institute of Physics, Helsinki, Finland
E. Anttila, S. Czellar, J. Härkönen, A. Heikkinen, V. Karimäki, R. Kinnunen, J. Klem, M.J. Kortelainen, T. Lampén, K. Lassila-Perini, S. Lehti, T. Lindén, P. Luukka, T. Mäenpää, J. Nysten, E. Tuominen, J. Tuominiemi, D. Ungaro, L. Wendland

Lappeenranta University of Technology, Lappeenranta, Finland
K. Banzuzi, A. Korpela, T. Tuuva

Laboratoire d'Annecy-le-Vieux de Physique des Particules, IN2P3-CNRS, Annecy-le-Vieux, France
P. Nedelec, D. Sillou

DSM/IRFU, CEA/Saclay, Gif-sur-Yvette, France
M. Besancon, R. Chipaux, M. Dejardin, D. Denegri, J. Descamps, B. Fabbro, J.L. Faure, F. Ferri, S. Ganjour, F.X. Gentit, A. Givernaud, P. Gras, G. Hamel de Monchenault, P. Jarry, M.C. Lemaire, E. Locci, J. Malcles, M. Marionneau, L. Millischer, J. Rander, A. Rosowsky, D. Rousseau, M. Titov, P. Verrecchia

Laboratoire Leprince-Ringuet, Ecole Polytechnique, IN2P3-CNRS, Palaiseau, France
S. Baffioni, L. Bianchini, M. Bluj[3], P. Busson, C. Charlot, L. Dobrzynski, R. Granier de Cassagnac, M. Haguenauer, P. Miné, P. Paganini, Y. Sirois, C. Thiebaux, A. Zabi

Institut Pluridisciplinaire Hubert Curien, Université de Strasbourg, Université de Haute Alsace Mulhouse, CNRS/IN2P3, Strasbourg, France
J.-L. Agram[4], A. Besson, D. Bloch, D. Bodin, J.-M. Brom, E. Conte[4], F. Drouhin[4], J.-C. Fontaine[4], D. Gelé, U. Goerlach, L. Gross, P. Juillot, A.-C. Le Bihan, Y. Patois, J. Speck, P. Van Hove

Université de Lyon, Université Claude Bernard Lyon 1, CNRS-IN2P3, Institut de Physique Nucléaire de Lyon, Villeurbanne, France
C. Baty, M. Bedjidian, J. Blaha, G. Boudoul, H. Brun, N. Chanon, R. Chierici, D. Contardo, P. Depasse, T. Dupasquier, H. El Mamouni, F. Fassi[5], J. Fay, S. Gascon, B. Ille, T. Kurca, T. Le Grand, M. Lethuillier, N. Lumb, L. Mirabito, S. Perries, M. Vander Donckt, P. Verdier

E. Andronikashvili Institute of Physics, Academy of Science, Tbilisi, Georgia
N. Djaoshvili, N. Roinishvili, V. Roinishvili

Institute of High Energy Physics and Informatization, Tbilisi State University, Tbilisi, Georgia
N. Amaglobeli

RWTH Aachen University, I. Physikalisches Institut, Aachen, Germany
R. Adolphi, G. Anagnostou, R. Brauer, W. Braunschweig, M. Edelhoff, H. Esser, L. Feld, W. Karpinski, A. Khomich, K. Klein, N. Mohr, A. Ostaptchouk, D. Pandoulas, G. Pierschel, F. Raupach, S. Schael, A. Schultz von Dratzig, G. Schwering, D. Sprenger, M. Thomas, M. Weber, B. Wittmer, M. Wlochal

RWTH Aachen University, III. Physikalisches Institut A, Aachen, Germany
O. Actis, G. Altenhöfer, W. Bender, P. Biallass, M. Erdmann, G. Fetchenhauer[1], J. Frangenheim, T. Hebbeker, G. Hilgers, A. Hinzmann, K. Hoepfner, C. Hof, M. Kirsch, T. Klimkovich, P. Kreuzer[1], D. Lanske[†], M. Merschmeyer, A. Meyer, B. Philipps, H. Pieta, H. Reithler, S.A. Schmitz, L. Sonnenschein, M. Sowa, J. Steggemann, H. Szczesny, D. Teyssier, C. Zeidler

RWTH Aachen University, III. Physikalisches Institut B, Aachen, Germany
M. Bontenackels, M. Davids, M. Duda, G. Flügge, H. Geenen, M. Giffels, W. Haj Ahmad, T. Hermanns, D. Heydhausen, S. Kalinin, T. Kress, A. Linn, A. Nowack, L. Perchalla, M. Poettgens, O. Pooth, P. Sauerland, A. Stahl, D. Tornier, M.H. Zoeller

Deutsches Elektronen-Synchrotron, Hamburg, Germany
M. Aldaya Martin, U. Behrens, K. Borras, A. Campbell, E. Castro, D. Dammann, G. Eckerlin, A. Flossdorf, G. Flucke, A. Geiser, D. Hatton, J. Hauk, H. Jung, M. Kasemann, I. Katkov, C. Kleinwort, H. Kluge, A. Knutsson, E. Kuznetsova, W. Lange, W. Lohmann, R. Mankel[1], M. Marienfeld, A.B. Meyer, S. Miglioranzi, J. Mnich, M. Ohlerich, J. Olzem, A. Parenti, C. Rosemann, R. Schmidt, T. Schoerner-Sadenius, D. Volyanskyy, C. Wissing, W.D. Zeuner[1]

University of Hamburg, Hamburg, Germany
C. Autermann, F. Bechtel, J. Draeger, D. Eckstein, U. Gebbert, K. Kaschube, G. Kaussen, R. Klanner, B. Mura, S. Naumann-Emme, F. Nowak, U. Pein, C. Sander, P. Schleper, T. Schum, H. Stadie, G. Steinbrück, J. Thomsen, R. Wolf

Institut für Experimentelle Kernphysik, Karlsruhe, Germany
J. Bauer, P. Blüm, V. Buege, A. Cakir, T. Chwalek, W. De Boer, A. Dierlamm, G. Dirkes, M. Feindt, U. Felzmann, M. Frey, A. Furgeri, J. Gruschke, C. Hackstein, F. Hartmann[1], S. Heier, M. Heinrich, H. Held, D. Hirschbuehl, K.H. Hoffmann, S. Honc, C. Jung, T. Kuhr, T. Liamsuwan, D. Martschei, S. Mueller, Th. Müller, M.B. Neuland, M. Niegel, O. Oberst, A. Oehler, J. Ott, T. Peiffer, D. Piparo, G. Quast, K. Rabbertz, F. Ratnikov, N. Ratnikova, M. Renz, C. Saout[1], G. Sartisohn, A. Scheurer, P. Schieferdecker, F.-P. Schilling, G. Schott, H.J. Simonis,

F.M. Stober, P. Sturm, D. Troendle, A. Trunov, W. Wagner, J. Wagner-Kuhr, M. Zeise, V. Zhukov[6], E.B. Ziebarth

Institute of Nuclear Physics "Demokritos", Aghia Paraskevi, Greece
G. Daskalakis, T. Geralis, K. Karafasoulis, A. Kyriakis, D. Loukas, A. Markou, C. Markou, C. Mavrommatis, E. Petrakou, A. Zachariadou

University of Athens, Athens, Greece
L. Gouskos, P. Katsas, A. Panagiotou[1]

University of Ioánnina, Ioánnina, Greece
I. Evangelou, P. Kokkas, N. Manthos, I. Papadopoulos, V. Patras, F.A. Triantis

KFKI Research Institute for Particle and Nuclear Physics, Budapest, Hungary
G. Bencze[1], L. Boldizsar, G. Debreczeni, C. Hajdu[1], S. Hernath, P. Hidas, D. Horvath[7], K. Krajczar, A. Laszlo, G. Patay, F. Sikler, N. Toth, G. Vesztergombi

Institute of Nuclear Research ATOMKI, Debrecen, Hungary
N. Beni, G. Christian, J. Imrek, J. Molnar, D. Novak, J. Palinkas, G. Szekely, Z. Szillasi[1], K. Tokesi, V. Veszpremi

University of Debrecen, Debrecen, Hungary
A. Kapusi, G. Marian, P. Raics, Z. Szabo, Z.L. Trocsanyi, B. Ujvari, G. Zilizi

Panjab University, Chandigarh, India
S. Bansal, H.S. Bawa, S.B. Beri, V. Bhatnagar, M. Jindal, M. Kaur, R. Kaur, J.M. Kohli, M.Z. Mehta, N. Nishu, L.K. Saini, A. Sharma, A. Singh, J.B. Singh, S.P. Singh

University of Delhi, Delhi, India
S. Ahuja, S. Arora, S. Bhattacharya[8], S. Chauhan, B.C. Choudhary, P. Gupta, S. Jain, S. Jain, M. Jha, A. Kumar, K. Ranjan, R.K. Shivpuri, A.K. Srivastava

Bhabha Atomic Research Centre, Mumbai, India
R.K. Choudhury, D. Dutta, S. Kailas, S.K. Kataria, A.K. Mohanty, L.M. Pant, P. Shukla, A. Topkar

Tata Institute of Fundamental Research - EHEP, Mumbai, India
T. Aziz, M. Guchait[9], A. Gurtu, M. Maity[10], D. Majumder, G. Majumder, K. Mazumdar, A. Nayak, A. Saha, K. Sudhakar

Tata Institute of Fundamental Research - HECR, Mumbai, India
S. Banerjee, S. Dugad, N.K. Mondal

Institute for Studies in Theoretical Physics & Mathematics (IPM), Tehran, Iran
H. Arfaei, H. Bakhshiansohi, A. Fahim, A. Jafari, M. Mohammadi Najafabadi, A. Moshaii, S. Paktinat Mehdiabadi, S. Rouhani, B. Safarzadeh, M. Zeinali

University College Dublin, Dublin, Ireland
M. Felcini

INFN Sezione di Bari [a], Università di Bari [b], Politecnico di Bari [c], Bari, Italy
M. Abbrescia[a,b], L. Barbone[a], F. Chiumarulo[a], A. Clemente[a], A. Colaleo[a], D. Creanza[a,c], G. Cuscela[a], N. De Filippis[a], M. De Palma[a,b], G. De Robertis[a], G. Donvito[a], F. Fedele[a], L. Fiore[a], M. Franco[a], G. Iaselli[a,c], N. Lacalamita[a], F. Loddo[a], L. Lusito[a,b], G. Maggi[a,c], M. Maggi[a], N. Manna[a,b], B. Marangelli[a,b], S. My[a,c], S. Natali[a,b], S. Nuzzo[a,b], G. Papagni[a], S. Piccolomo[a], G.A. Pierro[a], C. Pinto[a], A. Pompili[a,b], G. Pugliese[a,c], R. Rajan[a], A. Ranieri[a], F. Romano[a,c],

G. Roselli[a,b], G. Selvaggi[a,b], Y. Shinde[a], L. Silvestris[a], S. Tupputi[a,b], G. Zito[a]

INFN Sezione di Bologna [a], Universita di Bologna [b], Bologna, Italy
G. Abbiendi[a], W. Bacchi[a,b], A.C. Benvenuti[a], M. Boldini[a], D. Bonacorsi[a], S. Braibant-Giacomelli[a,b], V.D. Cafaro[a], S.S. Caiazza[a], P. Capiluppi[a,b], A. Castro[a,b], F.R. Cavallo[a], G. Codispoti[a,b], M. Cuffiani[a,b], I. D'Antone[a], G.M. Dallavalle[a,1], F. Fabbri[a], A. Fanfani[a,b], D. Fasanella[a], P. Giacomelli[a], V. Giordano[a], M. Giunta[a,1], C. Grandi[a], M. Guerzoni[a], S. Marcellini[a], G. Masetti[a,b], A. Montanari[a], F.L. Navarria[a,b], F. Odorici[a], G. Pellegrini[a], A. Perrotta[a], A.M. Rossi[a,b], T. Rovelli[a,b], G. Siroli[a,b], G. Torromeo[a], R. Travaglini[a,b]

INFN Sezione di Catania [a], Universita di Catania [b], Catania, Italy
S. Albergo[a,b], S. Costa[a,b], R. Potenza[a,b], A. Tricomi[a,b], C. Tuve[a]

INFN Sezione di Firenze [a], Universita di Firenze [b], Firenze, Italy
G. Barbagli[a], G. Broccolo[a,b], V. Ciulli[a,b], C. Civinini[a], R. D'Alessandro[a,b], E. Focardi[a,b], S. Frosali[a,b], E. Gallo[a], C. Genta[a,b], G. Landi[a,b], P. Lenzi[a,b,1], M. Meschini[a], S. Paoletti[a], G. Sguazzoni[a], A. Tropiano[a]

INFN Laboratori Nazionali di Frascati, Frascati, Italy
L. Benussi, M. Bertani, S. Bianco, S. Colafranceschi[11], D. Colonna[11], F. Fabbri, M. Giardoni, L. Passamonti, D. Piccolo, D. Pierluigi, B. Ponzio, A. Russo

INFN Sezione di Genova, Genova, Italy
P. Fabbricatore, R. Musenich

INFN Sezione di Milano-Biccoca [a], Universita di Milano-Bicocca [b], Milano, Italy
A. Benaglia[a], M. Calloni[a], G.B. Cerati[a,b,1], P. D'Angelo[a], F. De Guio[a], F.M. Farina[a], A. Ghezzi[a], P. Govoni[a,b], M. Malberti[a,b,1], S. Malvezzi[a], A. Martelli[a], D. Menasce[a], V. Miccio[a,b], L. Moroni[a], P. Negri[a,b], M. Paganoni[a,b], D. Pedrini[a], A. Pullia[a,b], S. Ragazzi[a,b], N. Redaelli[a], S. Sala[a], R. Salerno[a,b], T. Tabarelli de Fatis[a,b], V. Tancini[a,b], S. Taroni[a,b]

INFN Sezione di Napoli [a], Universita di Napoli "Federico II" [b], Napoli, Italy
S. Buontempo[a], N. Cavallo[a], A. Cimmino[a,b,1], M. De Gruttola[a,b,1], F. Fabozzi[a,12], A.O.M. Iorio[a], L. Lista[a], D. Lomidze[a], P. Noli[a,b], P. Paolucci[a], C. Sciacca[a,b]

INFN Sezione di Padova [a], Università di Padova [b], Padova, Italy
P. Azzi[a,1], N. Bacchetta[a], L. Barcellan[a], P. Bellan[a,b,1], M. Bellato[a], M. Benettoni[a], M. Biasotto[a,13], D. Bisello[a,b], E. Borsato[a,b], A. Branca[a], R. Carlin[a,b], L. Castellani[a], P. Checchia[a], E. Conti[a], F. Dal Corso[a], M. De Mattia[a,b], T. Dorigo[a], U. Dosselli[a], F. Fanzago[a], F. Gasparini[a,b], U. Gasparini[a,b], P. Giubilato[a,b], F. Gonella[a], A. Gresele[a,14], M. Gulmini[a,13], A. Kaminskiy[a,b], S. Lacaprara[a,13], I. Lazzizzera[a,14], M. Margoni[a,b], G. Maron[a,13], S. Mattiazzo[a,b], M. Mazzucato[a], M. Meneghelli[a], A.T. Meneguzzo[a,b], M. Michelotto[a], F. Montecassiano[a], M. Nespolo[a], M. Passaseo[a], M. Pegoraro[a], L. Perrozzi[a], N. Pozzobon[a,b], P. Ronchese[a,b], F. Simonetto[a,b], N. Toniolo[a], E. Torassa[a], M. Tosi[a,b], A. Triossi[a], S. Vanini[a,b], S. Ventura[a], P. Zotto[a,b], G. Zumerle[a,b]

INFN Sezione di Pavia [a], Universita di Pavia [b], Pavia, Italy
P. Baesso[a,b], U. Berzano[a], S. Bricola[a], M.M. Necchi[a,b], D. Pagano[a,b], S.P. Ratti[a,b], C. Riccardi[a,b], P. Torre[a,b], A. Vicini[a], P. Vitulo[a,b], C. Viviani[a,b]

INFN Sezione di Perugia [a], Universita di Perugia [b], Perugia, Italy
D. Aisa[a], S. Aisa[a], E. Babucci[a], M. Biasini[a,b], G.M. Bilei[a], B. Caponeri[a,b], B. Checcucci[a], N. Dinu[a], L. Fanò[a], L. Farnesini[a], P. Lariccia[a,b], A. Lucaroni[a,b], G. Mantovani[a,b], A. Nappi[a,b], A. Piluso[a], V. Postolache[a], A. Santocchia[a,b], L. Servoli[a], D. Tonoiu[a], A. Vedaee[a], R. Volpe[a,b]

INFN Sezione di Pisa ^{a}**, Universita di Pisa** ^{b}**, Scuola Normale Superiore di Pisa** ^{c}**, Pisa, Italy**
P. Azzurri^{a,c}, G. Bagliesi^a, J. Bernardini^{a,b}, L. Berretta^a, T. Boccali^a, A. Bocci^{a,c}, L. Borrello^{a,c}, F. Bosi^a, F. Calzolari^a, R. Castaldi^a, R. Dell'Orso^a, F. Fiori^{a,b}, L. Foà^{a,c}, S. Gennai^{a,c}, A. Giassi^a, A. Kraan^a, F. Ligabue^{a,c}, T. Lomtadze^a, F. Mariani^a, L. Martini^a, M. Massa^a, A. Messineo^{a,b}, A. Moggi^a, F. Palla^a, F. Palmonari^a, G. Petragnani^a, G. Petrucciani^{a,c}, F. Raffaelli^a, S. Sarkar^a, G. Segneri^a, A.T. Serban^a, P. Spagnolo^{a,1}, R. Tenchini^{a,1}, S. Tolaini^a, G. Tonelli^{a,b,1}, A. Venturi^a, P.G. Verdini^a

INFN Sezione di Roma ^{a}**, Universita di Roma "La Sapienza"** ^{b}**, Roma, Italy**
S. Baccaro^{a,15}, L. Barone^{a,b}, A. Bartoloni^a, F. Cavallari^{a,1}, I. Dafinei^a, D. Del Re^{a,b}, E. Di Marco^{a,b}, M. Diemoz^a, D. Franci^{a,b}, E. Longo^{a,b}, G. Organtini^{a,b}, A. Palma^{a,b}, F. Pandolfi^{a,b}, R. Paramatti^{a,1}, F. Pellegrino^a, S. Rahatlou^{a,b}, C. Rovelli^a

INFN Sezione di Torino ^{a}**, Università di Torino** ^{b}**, Università del Piemonte Orientale (Novara)** ^{c}**, Torino, Italy**
G. Alampi^a, N. Amapane^{a,b}, R. Arcidiacono^{a,b}, S. Argiro^{a,b}, M. Arneodo^{a,c}, C. Biino^a, M.A. Borgia^{a,b}, C. Botta^{a,b}, N. Cartiglia^a, R. Castello^{a,b}, G. Cerminara^{a,b}, M. Costa^{a,b}, D. Dattola^a, G. Dellacasa^a, N. Demaria^a, G. Dughera^a, F. Dumitrache^a, A. Graziano^{a,b}, C. Mariotti^a, M. Marone^{a,b}, S. Maselli^a, E. Migliore^{a,b}, G. Mila^{a,b}, V. Monaco^{a,b}, M. Musich^{a,b}, M. Nervo^{a,b}, M.M. Obertino^{a,c}, S. Oggero^{a,b}, R. Panero^a, N. Pastrone^a, M. Pelliccioni^{a,b}, A. Romero^{a,b}, M. Ruspa^{a,c}, R. Sacchi^{a,b}, A. Solano^{a,b}, A. Staiano^a, P.P. Trapani^{a,b,1}, D. Trocino^{a,b}, A. Vilela Pereira^{a,b}, L. Visca^{a,b}, A. Zampieri^a

INFN Sezione di Trieste ^{a}**, Universita di Trieste** ^{b}**, Trieste, Italy**
F. Ambroglini^{a,b}, S. Belforte^a, F. Cossutti^a, G. Della Ricca^{a,b}, B. Gobbo^a, A. Penzo^a

Kyungpook National University, Daegu, Korea
S. Chang, J. Chung, D.H. Kim, G.N. Kim, D.J. Kong, H. Park, D.C. Son

Wonkwang University, Iksan, Korea
S.Y. Bahk

Chonnam National University, Kwangju, Korea
S. Song

Konkuk University, Seoul, Korea
S.Y. Jung

Korea University, Seoul, Korea
B. Hong, H. Kim, J.H. Kim, K.S. Lee, D.H. Moon, S.K. Park, H.B. Rhee, K.S. Sim

Seoul National University, Seoul, Korea
J. Kim

University of Seoul, Seoul, Korea
M. Choi, G. Hahn, I.C. Park

Sungkyunkwan University, Suwon, Korea
S. Choi, Y. Choi, J. Goh, H. Jeong, T.J. Kim, J. Lee, S. Lee

Vilnius University, Vilnius, Lithuania
M. Janulis, D. Martisiute, P. Petrov, T. Sabonis

Centro de Investigacion y de Estudios Avanzados del IPN, Mexico City, Mexico
H. Castilla Valdez[1], A. Sánchez Hernández

Universidad Iberoamericana, Mexico City, Mexico
S. Carrillo Moreno

Universidad Autónoma de San Luis Potosí, San Luis Potosí, Mexico
A. Morelos Pineda

University of Auckland, Auckland, New Zealand
P. Allfrey, R.N.C. Gray, D. Krofcheck

University of Canterbury, Christchurch, New Zealand
N. Bernardino Rodrigues, P.H. Butler, T. Signal, J.C. Williams

National Centre for Physics, Quaid-I-Azam University, Islamabad, Pakistan
M. Ahmad, I. Ahmed, W. Ahmed, M.I. Asghar, M.I.M. Awan, H.R. Hoorani, I. Hussain,
W.A. Khan, T. Khurshid, S. Muhammad, S. Qazi, H. Shahzad

Institute of Experimental Physics, Warsaw, Poland
M. Cwiok, R. Dabrowski, W. Dominik, K. Doroba, M. Konecki, J. Krolikowski, K. Pozniak[16],
R. Romaniuk, W. Zabolotny[16], P. Zych

Soltan Institute for Nuclear Studies, Warsaw, Poland
T. Frueboes, R. Gokieli, L. Goscilo, M. Górski, M. Kazana, K. Nawrocki, M. Szleper, G. Wrochna,
P. Zalewski

Laboratório de Instrumentação e Física Experimental de Partículas, Lisboa, Portugal
N. Almeida, L. Antunes Pedro, P. Bargassa, A. David, P. Faccioli, P.G. Ferreira Parracho,
M. Freitas Ferreira, M. Gallinaro, M. Guerra Jordao, P. Martins, G. Mini, P. Musella, J. Pela,
L. Raposo, P.Q. Ribeiro, S. Sampaio, J. Seixas, J. Silva, P. Silva, D. Soares, M. Sousa, J. Varela,
H.K. Wöhri

Joint Institute for Nuclear Research, Dubna, Russia
I. Altsybeev, I. Belotelov, P. Bunin, Y. Ershov, I. Filozova, M. Finger, M. Finger Jr., A. Golunov,
I. Golutvin, N. Gorbounov, V. Kalagin, A. Kamenev, V. Karjavin, V. Konoplyanikov, V. Ko-
renkov, G. Kozlov, A. Kurenkov, A. Lanev, A. Makankin, V.V. Mitsyn, P. Moisenz, E. Nikonov,
D. Oleynik, V. Palichik, V. Perelygin, A. Petrosyan, R. Semenov, S. Shmatov, V. Smirnov,
D. Smolin, E. Tikhonenko, S. Vasil'ev, A. Vishnevskiy, A. Volodko, A. Zarubin, V. Zhiltsov

Petersburg Nuclear Physics Institute, Gatchina (St Petersburg), Russia
N. Bondar, L. Chtchipounov, A. Denisov, Y. Gavrikov, G. Gavrilov, V. Golovtsov, Y. Ivanov,
V. Kim, V. Kozlov, P. Levchenko, G. Obrant, E. Orishchin, A. Petrunin, Y. Shcheglov, A. Shchet-
kovskiy, V. Sknar, I. Smirnov, V. Sulimov, V. Tarakanov, L. Uvarov, S. Vavilov, G. Velichko,
S. Volkov, A. Vorobyev

Institute for Nuclear Research, Moscow, Russia
Yu. Andreev, A. Anisimov, P. Antipov, A. Dermenev, S. Gninenko, N. Golubev, M. Kirsanov,
N. Krasnikov, V. Matveev, A. Pashenkov, V.E. Postoev, A. Solovey, A. Solovey, A. Toropin,
S. Troitsky

Institute for Theoretical and Experimental Physics, Moscow, Russia
A. Baud, V. Epshteyn, V. Gavrilov, N. Ilina, V. Kaftanov[†], V. Kolosov, M. Kossov[1], A. Krokhotin,
S. Kuleshov, A. Oulianov, G. Safronov, S. Semenov, I. Shreyber, V. Stolin, E. Vlasov, A. Zhokin

Moscow State University, Moscow, Russia
E. Boos, M. Dubinin[17], L. Dudko, A. Ershov, A. Gribushin, V. Klyukhin, O. Kodolova, I. Lokhtin,
S. Petrushanko, L. Sarycheva, V. Savrin, A. Snigirev, I. Vardanyan

P.N. Lebedev Physical Institute, Moscow, Russia
I. Dremin, M. Kirakosyan, N. Konovalova, S.V. Rusakov, A. Vinogradov

State Research Center of Russian Federation, Institute for High Energy Physics, Protvino, Russia
S. Akimenko, A. Artamonov, I. Azhgirey, S. Bitioukov, V. Burtovoy, V. Grishin[1], V. Kachanov, D. Konstantinov, V. Krychkine, A. Levine, I. Lobov, V. Lukanin, Y. Mel'nik, V. Petrov, R. Ryutin, S. Slabospitsky, A. Sobol, A. Sytine, L. Tourtchanovitch, S. Troshin, N. Tyurin, A. Uzunian, A. Volkov

Vinca Institute of Nuclear Sciences, Belgrade, Serbia
P. Adzic, M. Djordjevic, D. Jovanovic[18], D. Krpic[18], D. Maletic, J. Puzovic[18], N. Smiljkovic

Centro de Investigaciones Energéticas Medioambientales y Tecnológicas (CIEMAT), Madrid, Spain
M. Aguilar-Benitez, J. Alberdi, J. Alcaraz Maestre, P. Arce, J.M. Barcala, C. Battilana, C. Burgos Lazaro, J. Caballero Bejar, E. Calvo, M. Cardenas Montes, M. Cepeda, M. Cerrada, M. Chamizo Llatas, F. Clemente, N. Colino, M. Daniel, B. De La Cruz, A. Delgado Peris, C. Diez Pardos, C. Fernandez Bedoya, J.P. Fernández Ramos, A. Ferrando, J. Flix, M.C. Fouz, P. Garcia-Abia, A.C. Garcia-Bonilla, O. Gonzalez Lopez, S. Goy Lopez, J.M. Hernandez, M.I. Josa, J. Marin, G. Merino, J. Molina, A. Molinero, J.J. Navarrete, J.C. Oller, J. Puerta Pelayo, L. Romero, J. Santaolalla, C. Villanueva Munoz, C. Willmott, C. Yuste

Universidad Autónoma de Madrid, Madrid, Spain
C. Albajar, M. Blanco Otano, J.F. de Trocóniz, A. Garcia Raboso, J.O. Lopez Berengueres

Universidad de Oviedo, Oviedo, Spain
J. Cuevas, J. Fernandez Menendez, I. Gonzalez Caballero, L. Lloret Iglesias, H. Naves Sordo, J.M. Vizan Garcia

Instituto de Física de Cantabria (IFCA), CSIC-Universidad de Cantabria, Santander, Spain
I.J. Cabrillo, A. Calderon, S.H. Chuang, I. Diaz Merino, C. Diez Gonzalez, J. Duarte Campderros, M. Fernandez, G. Gomez, J. Gonzalez Sanchez, R. Gonzalez Suarez, C. Jorda, P. Lobelle Pardo, A. Lopez Virto, J. Marco, R. Marco, C. Martinez Rivero, P. Martinez Ruiz del Arbol, F. Matorras, T. Rodrigo, A. Ruiz Jimeno, L. Scodellaro, M. Sobron Sanudo, I. Vila, R. Vilar Cortabitarte

CERN, European Organization for Nuclear Research, Geneva, Switzerland
D. Abbaneo, E. Albert, M. Alidra, S. Ashby, E. Auffray, J. Baechler, P. Baillon, A.H. Ball, S.L. Bally, D. Barney, F. Beaudette[19], R. Bellan, D. Benedetti, G. Benelli, C. Bernet, P. Bloch, S. Bolognesi, M. Bona, J. Bos, N. Bourgeois, T. Bourrel, H. Breuker, K. Bunkowski, D. Campi, T. Camporesi, E. Cano, A. Cattai, J.P. Chatelain, M. Chauvey, T. Christiansen, J.A. Coarasa Perez, A. Conde Garcia, R. Covarelli, B. Curé, A. De Roeck, V. Delachenal, D. Deyrail, S. Di Vincenzo[20], S. Dos Santos, T. Dupont, L.M. Edera, A. Elliott-Peisert, M. Eppard, M. Favre, N. Frank, W. Funk, A. Gaddi, M. Gastal, M. Gateau, H. Gerwig, D. Gigi, K. Gill, D. Giordano, J.P. Girod, F. Glege, R. Gomez-Reino Garrido, R. Goudard, S. Gowdy, R. Guida, L. Guiducci, J. Gutleber, M. Hansen, C. Hartl, J. Harvey, B. Hegner, H.F. Hoffmann, A. Holzner, A. Honma, M. Huhtinen, V. Innocente, P. Janot, G. Le Godec, P. Lecoq, C. Leonidopoulos, R. Loos, C. Lourenço, A. Lyonnet, A. Macpherson, N. Magini, J.D. Maillefaud, G. Maire, T. Mäki, L. Malgeri, M. Mannelli, L. Masetti, F. Meijers, P. Meridiani, S. Mersi, E. Meschi, A. Meynet Cordonnier, R. Moser, M. Mulders, J. Mulon, M. Noy, A. Oh, G. Olesen, A. Onnela, T. Orimoto, L. Orsini, E. Perez, G. Perinic, J.F. Pernot, P. Petagna, P. Petiot, A. Petrilli, A. Pfeiffer, M. Pierini, M. Pimiä, R. Pintus, B. Pirollet, H. Postema, A. Racz, S. Ravat, S.B. Rew, J. Rodrigues Antunes,

G. Rolandi[21], M. Rovere, V. Ryjov, H. Sakulin, D. Samyn, H. Sauce, C. Schäfer, W.D. Schlatter, M. Schröder, C. Schwick, A. Sciaba, I. Segoni, A. Sharma, N. Siegrist, P. Siegrist, N. Sinanis, T. Sobrier, P. Sphicas[22], D. Spiga, M. Spiropulu[17], F. Stöckli, P. Traczyk, P. Tropea, J. Troska, A. Tsirou, L. Veillet, G.I. Veres, M. Voutilainen, P. Wertelaers, M. Zanetti

Paul Scherrer Institut, Villigen, Switzerland
W. Bertl, K. Deiters, W. Erdmann, K. Gabathuler, R. Horisberger, Q. Ingram, H.C. Kaestli, S. König, D. Kotlinski, U. Langenegger, F. Meier, D. Renker, T. Rohe, J. Sibille[23], A. Starodumov[24]

Institute for Particle Physics, ETH Zurich, Zurich, Switzerland
B. Betev, L. Caminada[25], Z. Chen, S. Cittolin, D.R. Da Silva Di Calafiori, S. Dambach[25], G. Dissertori, M. Dittmar, C. Eggel[25], J. Eugster, G. Faber, K. Freudenreich, C. Grab, A. Hervé, W. Hintz, P. Lecomte, P.D. Luckey, W. Lustermann, C. Marchica[25], P. Milenovic[26], F. Moortgat, A. Nardulli, F. Nessi-Tedaldi, L. Pape, F. Pauss, T. Punz, A. Rizzi, F.J. Ronga, L. Sala, A.K. Sanchez, M.-C. Sawley, V. Sordini, B. Stieger, L. Tauscher[†], A. Thea, K. Theofilatos, D. Treille, P. Trüb[25], M. Weber, L. Wehrli, J. Weng, S. Zelepoukine[27]

Universität Zürich, Zurich, Switzerland
C. Amsler, V. Chiochia, S. De Visscher, C. Regenfus, P. Robmann, T. Rommerskirchen, A. Schmidt, D. Tsirigkas, L. Wilke

National Central University, Chung-Li, Taiwan
Y.H. Chang, E.A. Chen, W.T. Chen, A. Go, C.M. Kuo, S.W. Li, W. Lin

National Taiwan University (NTU), Taipei, Taiwan
P. Bartalini, P. Chang, Y. Chao, K.F. Chen, W.-S. Hou, Y. Hsiung, Y.J. Lei, S.W. Lin, R.-S. Lu, J. Schümann, J.G. Shiu, Y.M. Tzeng, K. Ueno, Y. Velikzhanin, C.C. Wang, M. Wang

Cukurova University, Adana, Turkey
A. Adiguzel, A. Ayhan, A. Azman Gokce, M.N. Bakirci, S. Cerci, I. Dumanoglu, E. Eskut, S. Girgis, E. Gurpinar, I. Hos, T. Karaman, T. Karaman, A. Kayis Topaksu, P. Kurt, G. Önengüt, G. Önengüt Gökbulut, K. Ozdemir, S. Ozturk, A. Polatöz, K. Sogut[28], B. Tali, H. Topakli, D. Uzun, L.N. Vergili, M. Vergili

Middle East Technical University, Physics Department, Ankara, Turkey
I.V. Akin, T. Aliev, S. Bilmis, M. Deniz, H. Gamsizkan, A.M. Guler, K. Öcalan, M. Serin, R. Sever, U.E. Surat, M. Zeyrek

Bogaziçi University, Department of Physics, Istanbul, Turkey
M. Deliomeroglu, D. Demir[29], E. Gülmez, A. Halu, B. Isildak, M. Kaya[30], O. Kaya[30], S. Ozkorucuklu[31], N. Sonmez[32]

National Scientific Center, Kharkov Institute of Physics and Technology, Kharkov, Ukraine
L. Levchuk, S. Lukyanenko, D. Soroka, S. Zub

University of Bristol, Bristol, United Kingdom
F. Bostock, J.J. Brooke, T.L. Cheng, D. Cussans, R. Frazier, J. Goldstein, N. Grant, M. Hansen, G.P. Heath, H.F. Heath, C. Hill, B. Huckvale, J. Jackson, C.K. Mackay, S. Metson, D.M. Newbold[33], K. Nirunpong, V.J. Smith, J. Velthuis, R. Walton

Rutherford Appleton Laboratory, Didcot, United Kingdom
K.W. Bell, C. Brew, R.M. Brown, B. Camanzi, D.J.A. Cockerill, J.A. Coughlan, N.I. Geddes, K. Harder, S. Harper, B.W. Kennedy, P. Murray, C.H. Shepherd-Themistocleous, I.R. Tomalin, J.H. Williams[†], W.J. Womersley, S.D. Worm

Imperial College, University of London, London, United Kingdom
R. Bainbridge, G. Ball, J. Ballin, R. Beuselinck, O. Buchmuller, D. Colling, N. Cripps, G. Davies, M. Della Negra, C. Foudas, J. Fulcher, D. Futyan, G. Hall, J. Hays, G. Iles, G. Karapostoli, B.C. MacEvoy, A.-M. Magnan, J. Marrouche, J. Nash, A. Nikitenko[24], A. Papageorgiou, M. Pesaresi, K. Petridis, M. Pioppi[34], D.M. Raymond, N. Rompotis, A. Rose, M.J. Ryan, C. Seez, P. Sharp, G. Sidiropoulos[1], M. Stettler, M. Stoye, M. Takahashi, A. Tapper, C. Timlin, S. Tourneur, M. Vazquez Acosta, T. Virdee[1], S. Wakefield, D. Wardrope, T. Whyntie, M. Wingham

Brunel University, Uxbridge, United Kingdom
J.E. Cole, I. Goitom, P.R. Hobson, A. Khan, P. Kyberd, D. Leslie, C. Munro, I.D. Reid, C. Siamitros, R. Taylor, L. Teodorescu, I. Yaselli

Boston University, Boston, USA
T. Bose, M. Carleton, E. Hazen, A.H. Heering, A. Heister, J. St. John, P. Lawson, D. Lazic, D. Osborne, J. Rohlf, L. Sulak, S. Wu

Brown University, Providence, USA
J. Andrea, A. Avetisyan, S. Bhattacharya, J.P. Chou, D. Cutts, S. Esen, G. Kukartsev, G. Landsberg, M. Narain, D. Nguyen, T. Speer, K.V. Tsang

University of California, Davis, Davis, USA
R. Breedon, M. Calderon De La Barca Sanchez, M. Case, D. Cebra, M. Chertok, J. Conway, P.T. Cox, J. Dolen, R. Erbacher, E. Friis, W. Ko, A. Kopecky, R. Lander, A. Lister, H. Liu, S. Maruyama, T. Miceli, M. Nikolic, D. Pellett, J. Robles, M. Searle, J. Smith, M. Squires, J. Stilley, M. Tripathi, R. Vasquez Sierra, C. Veelken

University of California, Los Angeles, Los Angeles, USA
V. Andreev, K. Arisaka, D. Cline, R. Cousins, S. Erhan[1], J. Hauser, M. Ignatenko, C. Jarvis, J. Mumford, C. Plager, G. Rakness, P. Schlein[†], J. Tucker, V. Valuev, R. Wallny, X. Yang

University of California, Riverside, Riverside, USA
J. Babb, M. Bose, A. Chandra, R. Clare, J.A. Ellison, J.W. Gary, G. Hanson, G.Y. Jeng, S.C. Kao, F. Liu, H. Liu, A. Luthra, H. Nguyen, G. Pasztor[35], A. Satpathy, B.C. Shen[†], R. Stringer, J. Sturdy, V. Sytnik, R. Wilken, S. Wimpenny

University of California, San Diego, La Jolla, USA
J.G. Branson, E. Dusinberre, D. Evans, F. Golf, R. Kelley, M. Lebourgeois, J. Letts, E. Lipeles, B. Mangano, J. Muelmenstaedt, M. Norman, S. Padhi, A. Petrucci, H. Pi, M. Pieri, R. Ranieri, M. Sani, V. Sharma, S. Simon, F. Würthwein, A. Yagil

University of California, Santa Barbara, Santa Barbara, USA
C. Campagnari, M. D'Alfonso, T. Danielson, J. Garberson, J. Incandela, C. Justus, P. Kalavase, S.A. Koay, D. Kovalskyi, V. Krutelyov, J. Lamb, S. Lowette, V. Pavlunin, F. Rebassoo, J. Ribnik, J. Richman, R. Rossin, D. Stuart, W. To, J.R. Vlimant, M. Witherell

California Institute of Technology, Pasadena, USA
A. Apresyan, A. Bornheim, J. Bunn, M. Chiorboli, M. Gataullin, D. Kcira, V. Litvine, Y. Ma, H.B. Newman, C. Rogan, V. Timciuc, J. Veverka, R. Wilkinson, Y. Yang, L. Zhang, K. Zhu, R.Y. Zhu

Carnegie Mellon University, Pittsburgh, USA
B. Akgun, R. Carroll, T. Ferguson, D.W. Jang, S.Y. Jun, M. Paulini, J. Russ, N. Terentyev, H. Vogel, I. Vorobiev

University of Colorado at Boulder, Boulder, USA
J.P. Cumalat, M.E. Dinardo, B.R. Drell, W.T. Ford, B. Heyburn, E. Luiggi Lopez, U. Nauenberg, K. Stenson, K. Ulmer, S.R. Wagner, S.L. Zang

Cornell University, Ithaca, USA
L. Agostino, J. Alexander, F. Blekman, D. Cassel, A. Chatterjee, S. Das, L.K. Gibbons, B. Heltsley, W. Hopkins, A. Khukhunaishvili, B. Kreis, V. Kuznetsov, J.R. Patterson, D. Puigh, A. Ryd, X. Shi, S. Stroiney, W. Sun, W.D. Teo, J. Thom, J. Vaughan, Y. Weng, P. Wittich

Fairfield University, Fairfield, USA
C.P. Beetz, G. Cirino, C. Sanzeni, D. Winn

Fermi National Accelerator Laboratory, Batavia, USA
S. Abdullin, M.A. Afaq[1], M. Albrow, B. Ananthan, G. Apollinari, M. Atac, W. Badgett, L. Bagby, J.A. Bakken, B. Baldin, S. Banerjee, K. Banicz, L.A.T. Bauerdick, A. Beretvas, J. Berryhill, P.C. Bhat, K. Biery, M. Binkley, I. Bloch, F. Borcherding, A.M. Brett, K. Burkett, J.N. Butler, V. Chetluru, H.W.K. Cheung, F. Chlebana, I. Churin, S. Cihangir, M. Crawford, W. Dagenhart, M. Demarteau, G. Derylo, D. Dykstra, D.P. Eartly, J.E. Elias, V.D. Elvira, D. Evans, L. Feng, M. Fischler, I. Fisk, S. Foulkes, J. Freeman, P. Gartung, E. Gottschalk, T. Grassi, D. Green, Y. Guo, O. Gutsche, A. Hahn, J. Hanlon, R.M. Harris, B. Holzman, J. Howell, D. Hufnagel, E. James, H. Jensen, M. Johnson, C.D. Jones, U. Joshi, E. Juska, J. Kaiser, B. Klima, S. Kossiakov, K. Kousouris, S. Kwan, C.M. Lei, P. Limon, J.A. Lopez Perez, S. Los, L. Lueking, G. Lukhanin, S. Lusin[1], J. Lykken, K. Maeshima, J.M. Marraffino, D. Mason, P. McBride, T. Miao, K. Mishra, S. Moccia, R. Mommsen, S. Mrenna, A.S. Muhammad, C. Newman-Holmes, C. Noeding, V. O'Dell, O. Prokofyev, R. Rivera, C.H. Rivetta, A. Ronzhin, P. Rossman, S. Ryu, V. Sekhri, E. Sexton-Kennedy, I. Sfiligoi, S. Sharma, T.M. Shaw, D. Shpakov, E. Skup, R.P. Smith[†], A. Soha, W.J. Spalding, L. Spiegel, I. Suzuki, P. Tan, W. Tanenbaum, S. Tkaczyk[1], R. Trentadue[1], L. Uplegger, E.W. Vaandering, R. Vidal, J. Whitmore, E. Wicklund, W. Wu, J. Yarba, F. Yumiceva, J.C. Yun

University of Florida, Gainesville, USA
D. Acosta, P. Avery, V. Barashko, D. Bourilkov, M. Chen, G.P. Di Giovanni, D. Dobur, A. Drozdetskiy, R.D. Field, Y. Fu, I.K. Furic, J. Gartner, D. Holmes, B. Kim, S. Klimenko, J. Konigsberg, A. Korytov, K. Kotov, A. Kropivnitskaya, T. Kypreos, A. Madorsky, K. Matchev, G. Mitselmakher, Y. Pakhotin, J. Piedra Gomez, C. Prescott, V. Rapsevicius, R. Remington, M. Schmitt, B. Scurlock, D. Wang, J. Yelton

Florida International University, Miami, USA
C. Ceron, V. Gaultney, L. Kramer, L.M. Lebolo, S. Linn, P. Markowitz, G. Martinez, J.L. Rodriguez

Florida State University, Tallahassee, USA
T. Adams, A. Askew, H. Baer, M. Bertoldi, J. Chen, W.G.D. Dharmaratna, S.V. Gleyzer, J. Haas, S. Hagopian, V. Hagopian, M. Jenkins, K.F. Johnson, E. Prettner, H. Prosper, S. Sekmen

Florida Institute of Technology, Melbourne, USA
M.M. Baarmand, S. Guragain, M. Hohlmann, H. Kalakhety, H. Mermerkaya, R. Ralich, I. Vodopiyanov

University of Illinois at Chicago (UIC), Chicago, USA
B. Abelev, M.R. Adams, I.M. Anghel, L. Apanasevich, V.E. Bazterra, R.R. Betts, J. Callner, M.A. Castro, R. Cavanaugh, C. Dragoiu, E.J. Garcia-Solis, C.E. Gerber, D.J. Hofman, S. Khalatian, C. Mironov, E. Shabalina, A. Smoron, N. Varelas

The University of Iowa, Iowa City, USA
U. Akgun, E.A. Albayrak, A.S. Ayan, B. Bilki, R. Briggs, K. Cankocak[36], K. Chung, W. Clarida, P. Debbins, F. Duru, F.D. Ingram, C.K. Lae, E. McCliment, J.-P. Merlo, A. Mestvirishvili, M.J. Miller, A. Moeller, J. Nachtman, C.R. Newsom, E. Norbeck, J. Olson, Y. Onel, F. Ozok, J. Parsons, I. Schmidt, S. Sen, J. Wetzel, T. Yetkin, K. Yi

Johns Hopkins University, Baltimore, USA
B.A. Barnett, B. Blumenfeld, A. Bonato, C.Y. Chien, D. Fehling, G. Giurgiu, A.V. Gritsan, Z.J. Guo, P. Maksimovic, S. Rappoccio, M. Swartz, N.V. Tran, Y. Zhang

The University of Kansas, Lawrence, USA
P. Baringer, A. Bean, O. Grachov, M. Murray, V. Radicci, S. Sanders, J.S. Wood, V. Zhukova

Kansas State University, Manhattan, USA
D. Bandurin, T. Bolton, K. Kaadze, A. Liu, Y. Maravin, D. Onoprienko, I. Svintradze, Z. Wan

Lawrence Livermore National Laboratory, Livermore, USA
J. Gronberg, J. Hollar, D. Lange, D. Wright

University of Maryland, College Park, USA
D. Baden, R. Bard, M. Boutemeur, S.C. Eno, D. Ferencek, N.J. Hadley, R.G. Kellogg, M. Kirn, S. Kunori, K. Rossato, P. Rumerio, F. Santanastasio, A. Skuja, J. Temple, M.B. Tonjes, S.C. Tonwar, T. Toole, E. Twedt

Massachusetts Institute of Technology, Cambridge, USA
B. Alver, G. Bauer, J. Bendavid, W. Busza, E. Butz, I.A. Cali, M. Chan, D. D'Enterria, P. Everaerts, G. Gomez Ceballos, K.A. Hahn, P. Harris, S. Jaditz, Y. Kim, M. Klute, Y.-J. Lee, W. Li, C. Loizides, T. Ma, M. Miller, S. Nahn, C. Paus, C. Roland, G. Roland, M. Rudolph, G. Stephans, K. Sumorok, K. Sung, S. Vaurynovich, E.A. Wenger, B. Wyslouch, S. Xie, Y. Yilmaz, A.S. Yoon

University of Minnesota, Minneapolis, USA
D. Bailleux, S.I. Cooper, P. Cushman, B. Dahmes, A. De Benedetti, A. Dolgopolov, P.R. Dudero, R. Egeland, G. Franzoni, J. Haupt, A. Inyakin[37], K. Klapoetke, Y. Kubota, J. Mans, N. Mirman, D. Petyt, V. Rekovic, R. Rusack, M. Schroeder, A. Singovsky, J. Zhang

University of Mississippi, University, USA
L.M. Cremaldi, R. Godang, R. Kroeger, L. Perera, R. Rahmat, D.A. Sanders, P. Sonnek, D. Summers

University of Nebraska-Lincoln, Lincoln, USA
K. Bloom, B. Bockelman, S. Bose, J. Butt, D.R. Claes, A. Dominguez, M. Eads, J. Keller, T. Kelly, I. Kravchenko, J. Lazo-Flores, C. Lundstedt, H. Malbouisson, S. Malik, G.R. Snow

State University of New York at Buffalo, Buffalo, USA
U. Baur, I. Iashvili, A. Kharchilava, A. Kumar, K. Smith, M. Strang

Northeastern University, Boston, USA
G. Alverson, E. Barberis, O. Boeriu, G. Eulisse, G. Govi, T. McCauley, Y. Musienko[38], S. Muzaffar, I. Osborne, T. Paul, S. Reucroft, J. Swain, L. Taylor, L. Tuura

Northwestern University, Evanston, USA
A. Anastassov, B. Gobbi, A. Kubik, R.A. Ofierzynski, A. Pozdnyakov, M. Schmitt, S. Stoynev, M. Velasco, S. Won

University of Notre Dame, Notre Dame, USA
L. Antonelli, D. Berry, M. Hildreth, C. Jessop, D.J. Karmgard, T. Kolberg, K. Lannon, S. Lynch,

N. Marinelli, D.M. Morse, R. Ruchti, J. Slaunwhite, J. Warchol, M. Wayne

The Ohio State University, Columbus, USA
B. Bylsma, L.S. Durkin, J. Gilmore[39], J. Gu, P. Killewald, T.Y. Ling, G. Williams

Princeton University, Princeton, USA
N. Adam, E. Berry, P. Elmer, A. Garmash, D. Gerbaudo, V. Halyo, A. Hunt, J. Jones, E. Laird, D. Marlow, T. Medvedeva, M. Mooney, J. Olsen, P. Piroué, D. Stickland, C. Tully, J.S. Werner, T. Wildish, Z. Xie, A. Zuranski

University of Puerto Rico, Mayaguez, USA
J.G. Acosta, M. Bonnett Del Alamo, X.T. Huang, A. Lopez, H. Mendez, S. Oliveros, J.E. Ramirez Vargas, N. Santacruz, A. Zatzerklyany

Purdue University, West Lafayette, USA
E. Alagoz, E. Antillon, V.E. Barnes, G. Bolla, D. Bortoletto, A. Everett, A.F. Garfinkel, Z. Gecse, L. Gutay, N. Ippolito, M. Jones, O. Koybasi, A.T. Laasanen, N. Leonardo, C. Liu, V. Maroussov, P. Merkel, D.H. Miller, N. Neumeister, A. Sedov, I. Shipsey, H.D. Yoo, Y. Zheng

Purdue University Calumet, Hammond, USA
P. Jindal, N. Parashar

Rice University, Houston, USA
V. Cuplov, K.M. Ecklund, F.J.M. Geurts, J.H. Liu, D. Maronde, M. Matveev, B.P. Padley, R. Redjimi, J. Roberts, L. Sabbatini, A. Tumanov

University of Rochester, Rochester, USA
B. Betchart, A. Bodek, H. Budd, Y.S. Chung, P. de Barbaro, R. Demina, H. Flacher, Y. Gotra, A. Harel, S. Korjenevski, D.C. Miner, D. Orbaker, G. Petrillo, D. Vishnevskiy, M. Zielinski

The Rockefeller University, New York, USA
A. Bhatti, L. Demortier, K. Goulianos, K. Hatakeyama, G. Lungu, C. Mesropian, M. Yan

Rutgers, the State University of New Jersey, Piscataway, USA
O. Atramentov, E. Bartz, Y. Gershtein, E. Halkiadakis, D. Hits, A. Lath, K. Rose, S. Schnetzer, S. Somalwar, R. Stone, S. Thomas, T.L. Watts

University of Tennessee, Knoxville, USA
G. Cerizza, M. Hollingsworth, S. Spanier, Z.C. Yang, A. York

Texas A&M University, College Station, USA
J. Asaadi, A. Aurisano, R. Eusebi, A. Golyash, A. Gurrola, T. Kamon, C.N. Nguyen, J. Pivarski, A. Safonov, S. Sengupta, D. Toback, M. Weinberger

Texas Tech University, Lubbock, USA
N. Akchurin, L. Berntzon, K. Gumus, C. Jeong, H. Kim, S.W. Lee, S. Popescu, Y. Roh, A. Sill, I. Volobouev, E. Washington, R. Wigmans, E. Yazgan

Vanderbilt University, Nashville, USA
D. Engh, C. Florez, W. Johns, S. Pathak, P. Sheldon

University of Virginia, Charlottesville, USA
D. Andelin, M.W. Arenton, M. Balazs, S. Boutle, M. Buehler, S. Conetti, B. Cox, R. Hirosky, A. Ledovskoy, C. Neu, D. Phillips II, M. Ronquest, R. Yohay

Wayne State University, Detroit, USA
S. Gollapinni, K. Gunthoti, R. Harr, P.E. Karchin, M. Mattson, A. Sakharov

University of Wisconsin, Madison, USA
M. Anderson, M. Bachtis, J.N. Bellinger, D. Carlsmith, I. Crotty[1], S. Dasu, S. Dutta, J. Efron, F. Feyzi, K. Flood, L. Gray, K.S. Grogg, M. Grothe, R. Hall-Wilton[1], M. Jaworski, P. Klabbers, J. Klukas, A. Lanaro, C. Lazaridis, J. Leonard, R. Loveless, M. Magrans de Abril, A. Mohapatra, G. Ott, G. Polese, D. Reeder, A. Savin, W.H. Smith, A. Sourkov[40], J. Swanson, M. Weinberg, D. Wenman, M. Wensveen, A. White

†: Deceased
1: Also at CERN, European Organization for Nuclear Research, Geneva, Switzerland
2: Also at Universidade Federal do ABC, Santo Andre, Brazil
3: Also at Soltan Institute for Nuclear Studies, Warsaw, Poland
4: Also at Université de Haute-Alsace, Mulhouse, France
5: Also at Centre de Calcul de l'Institut National de Physique Nucleaire et de Physique des Particules (IN2P3), Villeurbanne, France
6: Also at Moscow State University, Moscow, Russia
7: Also at Institute of Nuclear Research ATOMKI, Debrecen, Hungary
8: Also at University of California, San Diego, La Jolla, USA
9: Also at Tata Institute of Fundamental Research - HECR, Mumbai, India
10: Also at University of Visva-Bharati, Santiniketan, India
11: Also at Facolta' Ingegneria Universita' di Roma "La Sapienza", Roma, Italy
12: Also at Università della Basilicata, Potenza, Italy
13: Also at Laboratori Nazionali di Legnaro dell' INFN, Legnaro, Italy
14: Also at Università di Trento, Trento, Italy
15: Also at ENEA - Casaccia Research Center, S. Maria di Galeria, Italy
16: Also at Warsaw University of Technology, Institute of Electronic Systems, Warsaw, Poland
17: Also at California Institute of Technology, Pasadena, USA
18: Also at Faculty of Physics of University of Belgrade, Belgrade, Serbia
19: Also at Laboratoire Leprince-Ringuet, Ecole Polytechnique, IN2P3-CNRS, Palaiseau, France
20: Also at Alstom Contracting, Geneve, Switzerland
21: Also at Scuola Normale e Sezione dell' INFN, Pisa, Italy
22: Also at University of Athens, Athens, Greece
23: Also at The University of Kansas, Lawrence, USA
24: Also at Institute for Theoretical and Experimental Physics, Moscow, Russia
25: Also at Paul Scherrer Institut, Villigen, Switzerland
26: Also at Vinca Institute of Nuclear Sciences, Belgrade, Serbia
27: Also at University of Wisconsin, Madison, USA
28: Also at Mersin University, Mersin, Turkey
29: Also at Izmir Institute of Technology, Izmir, Turkey
30: Also at Kafkas University, Kars, Turkey
31: Also at Suleyman Demirel University, Isparta, Turkey
32: Also at Ege University, Izmir, Turkey
33: Also at Rutherford Appleton Laboratory, Didcot, United Kingdom
34: Also at INFN Sezione di Perugia; Universita di Perugia, Perugia, Italy
35: Also at KFKI Research Institute for Particle and Nuclear Physics, Budapest, Hungary
36: Also at Istanbul Technical University, Istanbul, Turkey
37: Also at University of Minnesota, Minneapolis, USA
38: Also at Institute for Nuclear Research, Moscow, Russia
39: Also at Texas A&M University, College Station, USA
40: Also at State Research Center of Russian Federation, Institute for High Energy Physics, Protvino, Russia